THE HYPERVELOCITY IMPACT OF PELLET WITH THIN PLATES: THEORETICAL CONSIDERATIONS

Part 2.

Report Rep. 62-8

by

W.H. Friend,
D.A. Millar,*
and
C.L. Murphy.

Department of Mechanical Engineering

McGill University

Montreal

October 1962

*Professor, Carleton University, and Consultant, Computing Devices of Canada Ltd.

ACKNOWLEDGEMENTS

This investigation of pellets impacting on thin plates was undertaken for the A.D. Little Company in support of their research program (Contract No. NAS5-664) for NASA, on fuel storage protection in space. The authors are indebted to many members of the A.D Little Company for valuable discussions and criticisms particularly Drs. N. Wiederhorn, R.H. Johnston and A.G. Emslie as well as Professor Sydney Goldstein of Harvard University.

Dr. Millar worked on this report as a consultant under an agreement with McGill University and Computing Devices of Canada.

The authors are indebted to Dr. G.V. Bull of McGill University whose initial work, inspiration, and supervision have made this report possible.

The authors thank Miss J. Lacroix for her efforts in typing the report.

TABLE OF CONTENTS

SUMMARY

18648

The theoretical analyses of the impact of pellets with thin plates and the resulting expansion flow is presented in this report. The analysis is based on the impact model discussed in reference 1, in which what are hoped to be secondary effects, are neglected. The short term expansion of the plasma, the interaction between shock and rarefaction waves, and the long term expansion are investigated in some detail.

Engineering design data for the protection of a space vehicle from meteor impacts are presented on the basis of the theoretical calculations carried out on the impact model.

Experimental procedures are outlined to check the theoretical results in the velocity range of 7 - 10 km/sec., which are obtainable in the laboratory. Further theoretical analyses are indicated which would allow for a more refined model and take temperature effects into account.

1.0 INTRODUCTION

The development of protective systems against meteoroid impacts for space vehicles cannot be carried out experimentally because meteoroid velocities exceed those attainable experimentally with macroscopic particles. In order to design a protection system, it is necessary to develop an analytical model which will allow prediction of impact effects, to check this model at velocities which are reliably attainable in the laboratory, and to hope that it will satisfactorily predict higher velocity effects. This hope can be realized only if the nature of the physical processes do not alter in the velocity regime of interest, that is from the 7 - 10 km/sec. of the laboratory, to the 72 km/sec. which is said to be the maximum meteoroid velocity (Ref. 4).

A series of changes does in fact take place in the impact processes in the velocity range from zero up to 5 km/sec, as the pressures generated range from those which produce only plastic deformation, up to those which vaporize and ionize the impacting materials.

Since the minimum meteoroid velocities are adequate to cause vaporization on impact, there is good reason to believe that a single model may be applicable over the entire range of meteoroid velocities unless the

astronomical temperatures and pressures generated in the higher range of impact velocities initiate fusion reactions with suitable materials, so introducing another physical process.

In 1946, Whipple (reference 11) suggested that the kinetic energy of a meteoroid could be used to destroy it on impact with a bumper, or shield, spaced a distance away from the main vehicle skin. The thickness of such a bumper might need to be only a fraction of the size of the meteoroid, provided the impact velocity and spacing were large.

This report and its predecessor (ref. 1) describe the analysis of a model for the end-on impact of a cylinder on a thin plate, assuming that the impact velocity is sufficient to vapourize the primary shocked region (figure 4.1). For most materials this means velocities exceeding about 10 km/sec., although a few would vapourize at about half this velocity.

The objective of the research program to be discussed in this report is the development for engineering design purposes, of an adequate method of predicting bumper plate effectiveness. The problem may be divided into various distinct phases. The first concerns the initial states generated by impact in both the bumper and the colliding particle. Confining our attention to the high velocity range of the spectrum associated with meteors, we may make the observation that the dominant phenomena are the impact generated shock waves which proceed ahead of any other

disturbance spreading throughout the bumper and colliding particle. This approach assumes the validity of classical fluid mechanics, and has been used extensively by workers at Los Alamos (refs. 2 and 3) to derive from measured shock wave characteristics, the appropriate equations of state for compressed metals, and by Bjork (ref. 4) and others for analyzing hypervelocity impact phenomena. In order to apply this relatively simple analytical model to impact, losses arising from fracture, vapourization, ignition etc. are neglected, and the shock assumed to behave as it would in an ideal medium with perhaps an additional complexity of a modified equation of state.

The conditions generated at the instant of impact, will be subsequently distributed in time quite differently depending on whether the processes are confined to one dimension or allowed to develop in a general three-dimensional manner. Bjork[4] employed a computer solution to obtain numerical answers to specific cases, while in order to obtain an insight into the role of various parameters a previous report (ref. 1) performed under this study contract assumed impact shocks of sufficient strength that the standard strong shock assumption of limiting density ratio could be made. These assumptions allowed quite simple analytical expressions to be developed for impact induced thermodynamic states.

The theoretical analysis so far completed has opened up a number of experimental avenues of approach to check the original theoretical model. Refinements and additional effects, such as ionization, can then be considered in a re-appraisal of the original theoretical model.

2.0 NOMENCLATURE

a - sound speed - mm/μsec (i.e. km/sec).

e - specific internal energy - kilocal/gm

P - pressure - megabars

$\overleftarrow{R}$ or $\overrightarrow{R}$ - left and right running rarefactions

$\downarrow R$ - inward running rarefaction

r - radius - mm., radial coordinate

$\overleftarrow{S}$ or $\overrightarrow{S}$ - left and right running shocks

S - entropy

t - time - sec. or μsec

T - temperature - ^{o}R or ^{o}K

u - element or particle velocity, relative to unshocked material. mm/μsec

V - pellet velocity, relative to bumper - mm/usec

v - particle velocity, absolute (relative to original bumper) mm/μsec

w - shock speed, relative to unshocked material, mm/μsec

x - axial coordinate, axial distance, mm.

δ - bumper thickness - mm.

γ - C_p/C_v or polytropic exponent

ρ - density gm/cm^3

σ $-\sqrt{\dfrac{\gamma_B+1}{\gamma_p+1}\dfrac{\rho_{B_o}}{\rho_{p_o}}}$

σ' $-\sqrt{\dfrac{\gamma_p+1}{\gamma_B+1}\cdot\dfrac{\rho_{p_o}}{\rho_{B_o}}}$

Subscripts

B - bumper

P - pellet

o - unshocked condition

A - axial

c - cylindrical

r - radial

3.0 APPLICATION TO VEHICLE ENGINEERING DESIGN

The information required by the engineer attempting to design a protection system for a space vehicle so that it will be able to complete its mission with an acceptably low probability of destruction by an impacting meteor is drawn from many branches of science and mathematics. To design a protection system that would be 100% reliable is virtually impossible, since he would require precise information regarding the characteristics of all meteors, their composition, mass, density, shape, velocity, and in particular their position in space at any time. In addition he would require knowledge of the real physical processes which occur when such a meteor impacted against some arbitrary bumper material so that he could construct the main vehicle hull to withstand the resulting forces exerted on it.

The information we have at our disposal is rather vague in nature and also somewhat uncertain. From observation of meteors entering the earth's atmosphere, and lately from information relayed to the ground by satellites in near earth orbits, astronomers and physicists have made order of magnitude predictions of the composition of meteors. These predictions vary, depending on source, from 5×10^{-2} gm/cc for the so-called dust-ball meteor to 2-10 gms/cc for the stony or metallic meteor. Reasonably

good agreement has been reached by scientists engaged in the prediction of the velocity range of meteors; it is generally conceded that most meteors have a velocity between 11 and 72 km per second with relatively large concentrations in the 20 km per second range and in the 40 km per second range. Other investigations indicate that meteors are not distributed uniformly in space, and in addition the size and velocity of meteors in dependent on position in space. It is expected that relatively small meteors, with $\rho \approx .05$ gm/cc. would be encountered on missions involving earth orbits; the majority of these would presumably be in orbit about the earth and hence their velocity could be predicted reasonably accurately. In addition to the random distribution of meteors in space, there appears to be a large concentration of meteors in certain regions within the solar system as demonstrated by the marked increase of the number of meteors entering the earth's atmosphere at particular times of the year. This zone of concentration appears to be in the plane containing the sun and the majority of the planets, with the numbers decreasing with distance from this plane.

This report does not attempt to provide the designer with the type of precise information he normally expects when asked to design a system to perform a particular

function with a high degree of reliability. It does, however, in the opinion of the authors, provide the best information available based on current knowledge of the meteor problem. Many assumptions and approximations have been made in the analysis leading to the design data presented here, some out of expedience in order to obtain early, albeit crude solutions, (i.e. the assumption of cylindrical meteors with their velocity vector along the axis of symmetry) and some out of necessity to make the problem tractable to analytical analysis, or to fill gaps in the present day knowledge of the complex physical processes occurring in the vapourization and expansion of materials undergoing hypervelocity impact.

To provide an adequate meteor protection device the designer must first decide on the characteristics of the "maximum acceptable" meteor; that is, he must decide on the size, density and velocity of the meteor he wishes to protect against. The probability of encountering a meteor of a particular size, density and velocity is dependent on the particular mission and size of the space craft; the protection system must be so designed that the chance of encountering a larger, faster or slower, or more dense meteor than that decided upon, which would penetrate the protection system, is consistent with the acceptable chance of failure of the mission.

Having chosen the characteristics of the meteor, i.e. the minimum velocity and maximum size and density which would likely be encountered, the information contained in figure 3.1, will give the minimum thickness necessary for a given bumper material to completely vaporize the impacting meteor. For the range of meteor's likely to be encountered it will be found that the bumper thickness will be limited by structural considerations in which case the minimum density of the bumper material can be determined from figure 3.1. The critical pressure below which the pellet or meteor material would not vaporize was taken to be approximately equal to 1.5×10^6 psi. This figure is well above the vapor pressure of most materials.

The polytropic exponent (γ) relating pressure and density of the vaporized meteor material was taken as 3, a value currently thought to be most representative of the highly shocked impact states.

Once the bumper material and thickness have been chosen to satisfy the conditions necessary to vaporize the meteor, the spacing of the bumper from the vehicle skin must be determined. The spacing will have to be large enough to permit the expansion of the highly compressed, highly energized plasma to an acceptably low pressure and energy level consistent with the design of the main vehicle hull. The spacing of the bumper then will depend on the

CRITICAL PELLET LENGTH vs PELLET KINETIC ENERGY

FOR VARIOUS DENSITY RATIOS $\rho_{B_0}/\rho_{P_0} = \sigma$

FOR $\gamma_B = \gamma_P = \gamma$

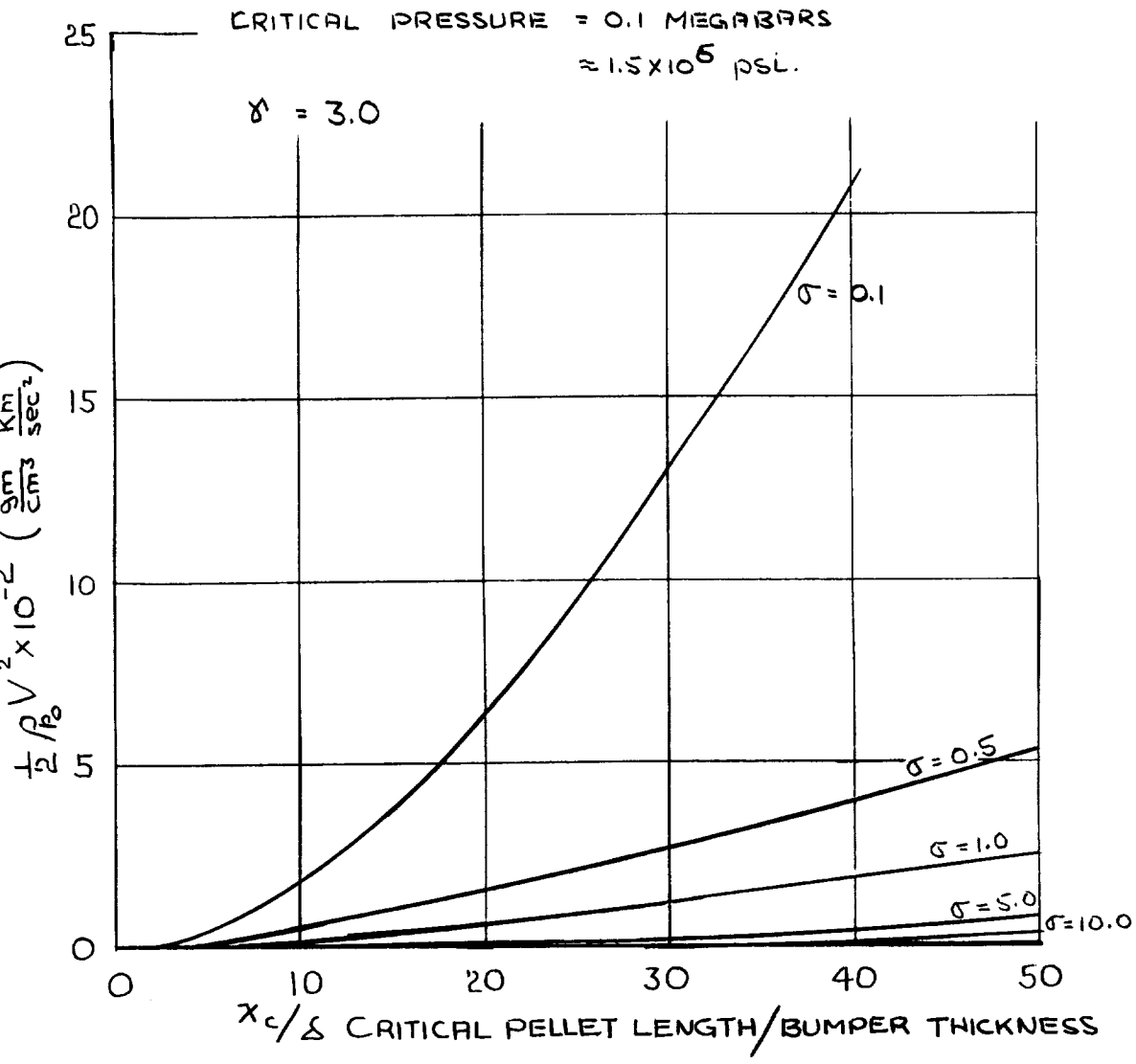

FIG. 3.1

capacity of the skin to absorb energy and impulsive pressure loading and on the residual energy, and pressure distribution in the "spray".

Figures 3.2 & 3.4 show the spacing that is required knowing the maximum velocity, density, and size of the meteor and the maximum pressure the skin can withstand at a point. If the rate at which the pressure is applied or the impact loading is the critical value this also can be obtained from the non-dimensional time coefficient $\frac{t}{s/V}$ of figure 3.2.

Figure 3.3 indicates that the radial distribution of pressure has a generally Gaussian shape, with the peak value equal to that predicted by figure 3.3 and decaying approximately as the inverse cube of the radius, measured from the line of flight of the meteor axis. The force exerted on the vehicle skin can then be determined by the integration of these curves and checked with design data. From these observations it is apparent that the maximum spacing should be used, thereby reducing the peak pressure and energy levels to a minimum at the vehicle skin. The choice of $\gamma = 3$ will give a conservative estimate of the spacing required both for maximum pressure and impact loading as it is likely that this choice of γ would be high for the vapourized material after a long term expansion.

EXPANDING SPHERE ANALYSIS FOR S > 2 DIAM.

CENTRE LINE PRESSURE COEFF. vs TIME COEFF.

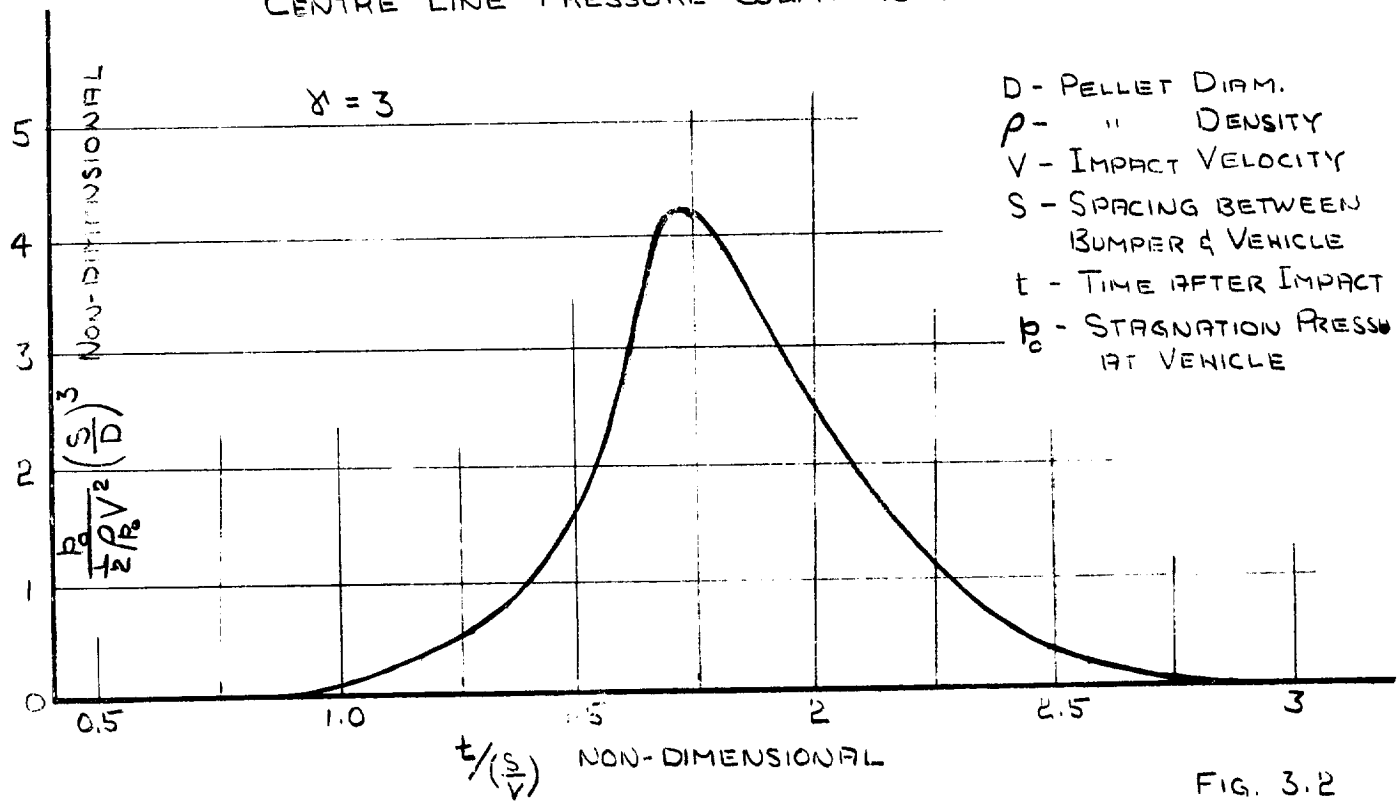

FIG. 3.2

PEAK PRESSURE PROFILES

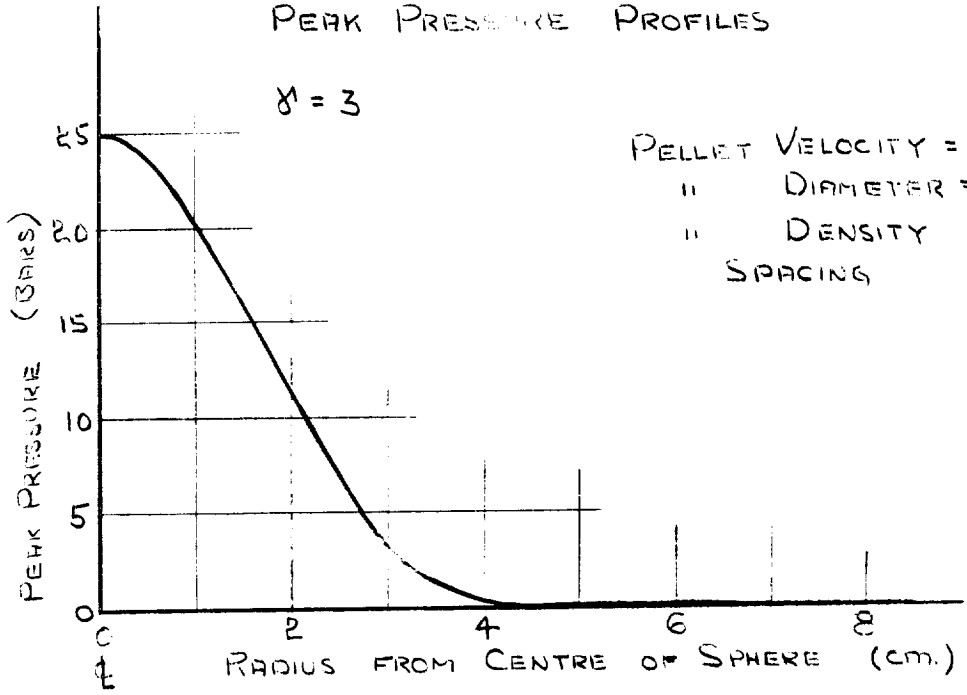

FIG. 3.3

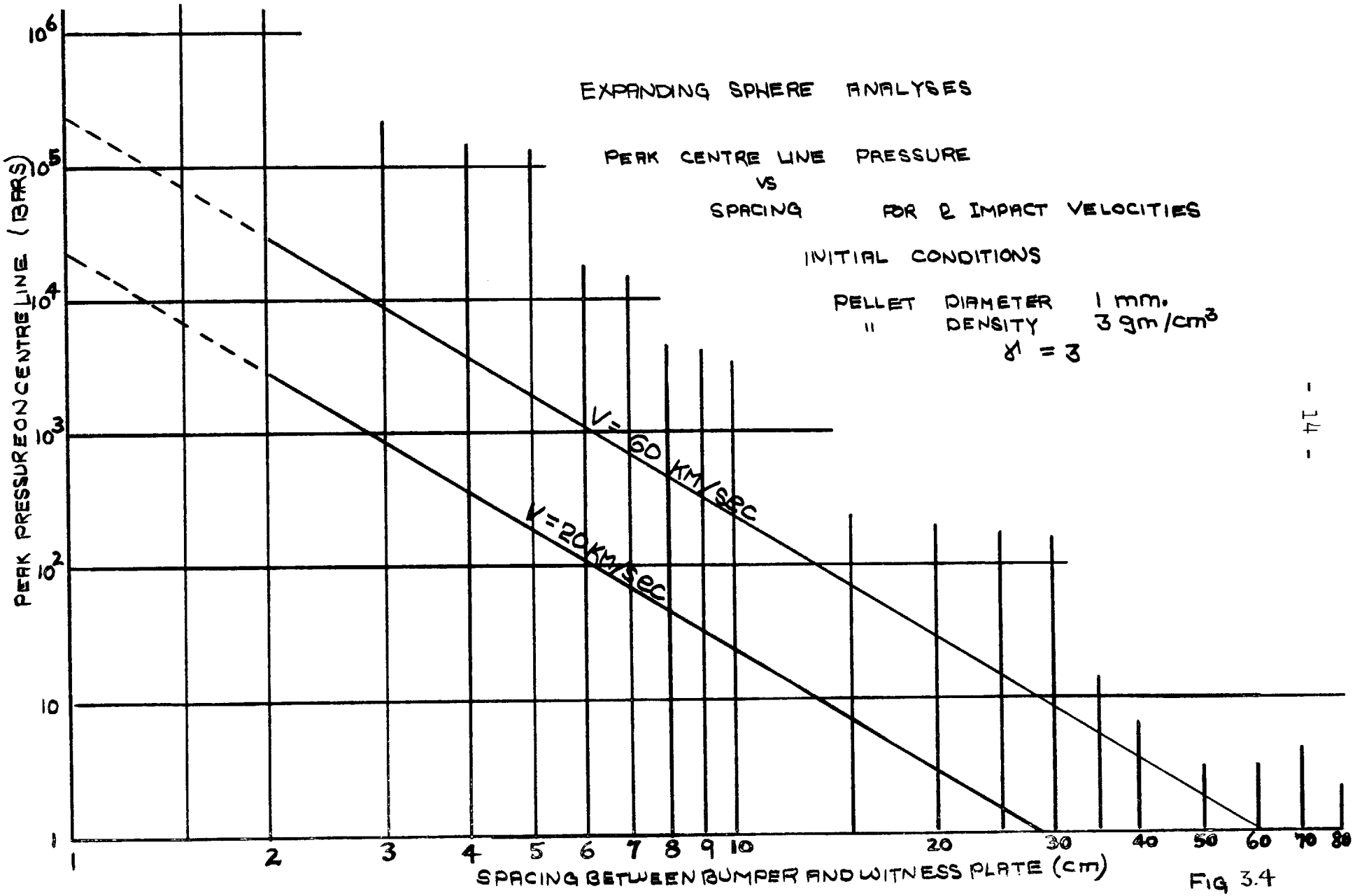
EXPANDING SPHERE ANALYSES
PEAK CENTRE LINE PRESSURE
VS
SPACING FOR 2 IMPACT VELOCITIES
INITIAL CONDITIONS
PELLET DIAMETER 1 mm.
" DENSITY 3 gm/cm³
γ = 3
V=60 KM/SEC
V=20 KM/SEC
PEAK PRESSURE ON CENTRE LINE (BARS)
SPACING BETWEEN BUMPER AND WITNESS PLATE (cm)
10⁶
10⁵
10⁴
10³
10²
10
1
1 2 3 4 5 6 7 8 9 10 20 30 40 50 60 70 80

Fig 3.4

The superficial nature of the simulation of the actual expansion by the model used makes the detail of the results calculated somewhat dubious, however, the spatial and temporal distribution is broadly speaking correct although the effect of the true nature of the complex decay systems will certainly influence the detailed shape of the curves. The assumption of uniform translation of the expanding sphere (at the initial velocity of the shocked media U_B) introduces an obvious error in the results since in general the total momentum delivered to the target as a consequence of this assumption will exceed that of the incoming meteor. If the incoming meteor shock vapourizes an amount of bumper material equal to its own initial mass the resulting expansion cloud would translate with a uniform velocity as assumed. However, in general, the mass of the shocked bumper material will be much less than that of the meteor, particularly if the "maximum acceptable" meteor is encountered, and hence a conservative error is introduced into the analysis. This conservative error would make the result more acceptable as design data.

4.0 GENERAL METHOD OF ANALYSIS

4.1 Initial Shock System

The impact of a particle with a bumper will produce a complex shock wave pattern in both materials, as the pellet is decelerated and the bumper material is accelerated. For analysis, this complex shock system is simplified (ref. 1) by considering the impact of a cylindrical pellet, end on, with a bumper much thinner than the pellet diameter. The shock system is then taken as one-dimensional within the bumper consisting of two plane shock waves, one in the pellet and another in the bumper, as shown in figure 4.2.1a.

The shock pressures, densities and velocities must satisfy the dynamic equations of motion; in addition, the compressed gas is assumed to obey the gas law $P = \rho RT$ and a polytropic relationship between pressure and density $P = A\rho^{\gamma}$. The application of standard analytical methods (refs. 9, 10) then leads to the Rankin-Hugoniot relations. If the strong shock density ratio is assumed $(\frac{\rho}{\rho_o} = \frac{\gamma+1}{\gamma-1})$, the following relationships can be shown (ref. 1) to exist.

a) Particle velocity behind the shock, relative to unshocked material.

$$u_B = \frac{V}{1+\sigma}, \quad \text{where } \sigma^2 = \frac{\gamma_B+1}{\gamma_P+1}\cdot\frac{\rho_{B_o}}{\rho_{P_o}} \qquad \ldots 4.1a$$

$$u_P = \sigma . u_B \qquad \ldots 4.1b$$

b) Shock velocity, relative to unshocked material

$$w_B = \frac{\gamma_B + 1}{2} u_B \; ; \quad w_P = \frac{\gamma_P + 1}{2} u_P \qquad \ldots 4.2a,b$$

c) Shock pressure, assuming $P_{B_o} = P_{P_o} = 0$

$$P_P = P_B = \frac{\gamma_B + 1}{2} . \rho_{B_o} . u_B \qquad \ldots 4.3a,b$$

d)
$$C_{V_B} T_B = \frac{u_B^2}{2} = \frac{R_B}{\gamma_B - 1} T_B \qquad \ldots 4.4a$$

$$C_{V_P} T_P = \frac{u_P^2}{2} = \frac{R_P}{\gamma_P - 1} T_P \qquad \ldots 4.4b$$

e) Sound speed in shocked material

$$a_B = \sqrt{\frac{\gamma_B(\gamma_B - 1)}{2} u_B} \qquad \ldots 4.5a$$

$$a_P = \sqrt{\frac{\gamma_P(\gamma_P - 1)}{2} u_P} \qquad \ldots 4.5b$$

The significance of particular values of γ can be shown by taking a few numerical examples. Consider $\gamma_B = \gamma_P$, $\rho_{B_o} = \rho_{P_o}$, hence $\sigma = 1$.

a) $\gamma \geqslant 3$. For $\gamma = 3$, $w_B = w_P = 2u_B = V$, so that the pellet shock moves upstream at the same speed as the pellet moves into the bumper, hence $\overleftarrow{S_p}$ remains in the plane of the upstream face of the bumper. For $\gamma > 3$, the shock velocity exceeds the pellet velocity and the shock moves upstream

of the bumper. For $\sigma < 1$ (bumper less dense than pellet), the same effect can be found for $\gamma < 3$.

b) $\gamma \leq 2$. For $\gamma \leq 2$, $a_B \leq u_B$, and the fluid flow is sonic or supersonic, so that rarefactions and small pressure waves cannot flow upstream. Since the bumper shock reflects at the bumper rear face as a rarefaction travelling upstream at a velocity equal to a_B, it will remain in the plane of the downstream face of the bumper for $\gamma = 2$, and be swept downstream for $\gamma < 2$. Since σ does not enter the relationship between a and u, its value does not alter these deductions.

c) $2 < \gamma < 3$. For values of γ between 2 and 3 the pellet shock will remain inside the bumper and be overtaken by the rarefaction wave. For $\sigma < 1$ the pellet shock will tend to move upstream of the bumper and for $\sigma > 1$ the pellet shock will tend to move downstream of the bumper.

4.2 Initial Expansion Process

The initial expansion process has been analysed assuming that the shock has not been decayed by the rarefaction waves. This imposes a limit for the time for the initial expansion processes to be valid. The nature of the initial expansion depends on the value of γ and σ.

For $(\frac{\sigma}{1+\sigma})\cdot\gamma < 1$ (assuming $\gamma_P = \gamma_B = \gamma$) the expansion flow takes place outside and downstream of the bumper. This case was considered in Ref. 1, and little further work has been done on it since that report was issued.

Figures 4.2.1b and c illustrate the type of expansion flow, and figure 4.2.2 gives the spray cone angle resulting from the expansion. The spray angle is given by the axial velocity of a particle (u_B) at the time it is given the radial escape velocity ($\frac{2}{\gamma-1}\cdot a_B$). This angle remains fixed (for strong shocks) since both u_B and a_B decrease by the same factor as the shock decays.

For values of $\gamma > 1 + \frac{1}{\sigma}$, the expansion process resembles the flow out of a nozzle or cavity, since the release wave can move into the subsonic stream of compressed medium. This material is enclosed by the walls of the hole in the bumper and is fed by the pellet shock as the pellet feeds into it. The arrival of the bumper shock at the rear face of the bumper completes the vaporization of the bumper; the shock reflects as a centered rarefaction wave (in the x-t plane) whose head moves into the compressed gas. This produces a jet or stream of gas downstream of the bumper. The extreme particle (forming the escape boundary and tail of the axial rarefaction) moving at escape velocity with zero temperature,

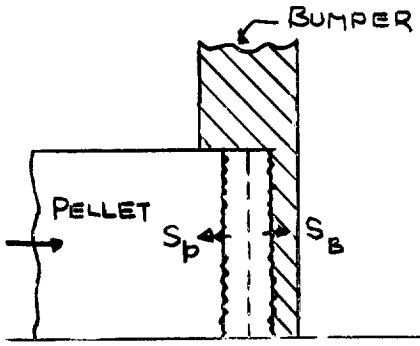

FIG. 4.2.1a SHOCKS STILL ENCLOSED IN BUMPER

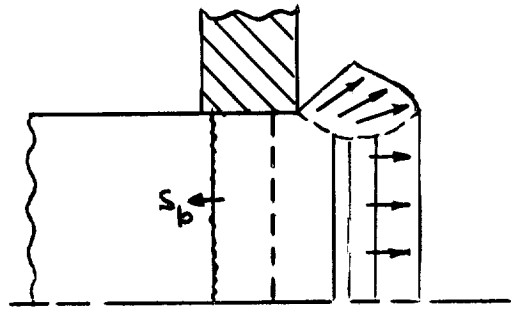

FIG 4.2.1b BUMPER SHOCK REFLECTED, PELLET SHOCK STILL ENCLOSED

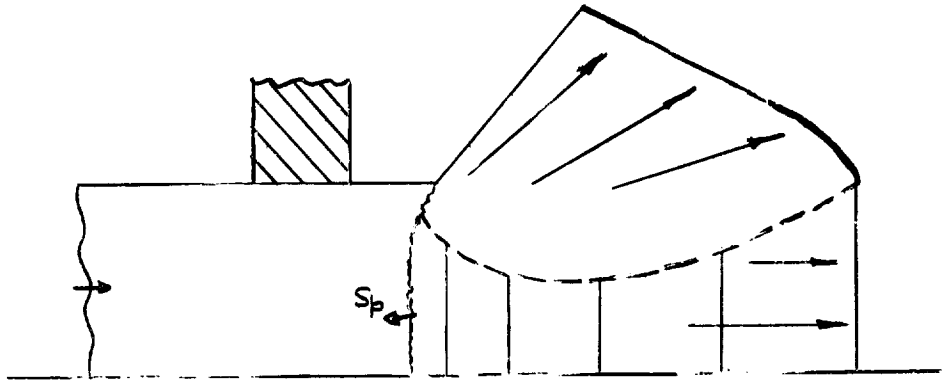

FIG 4.2.1c PELLET SHOCK OUTSIDE BUMPER, AND DECAYED BY AXIAL AND RADIAL RAREFACTION WAVES

RELEASED MODEL CONE SPRAY HALF ANGLES

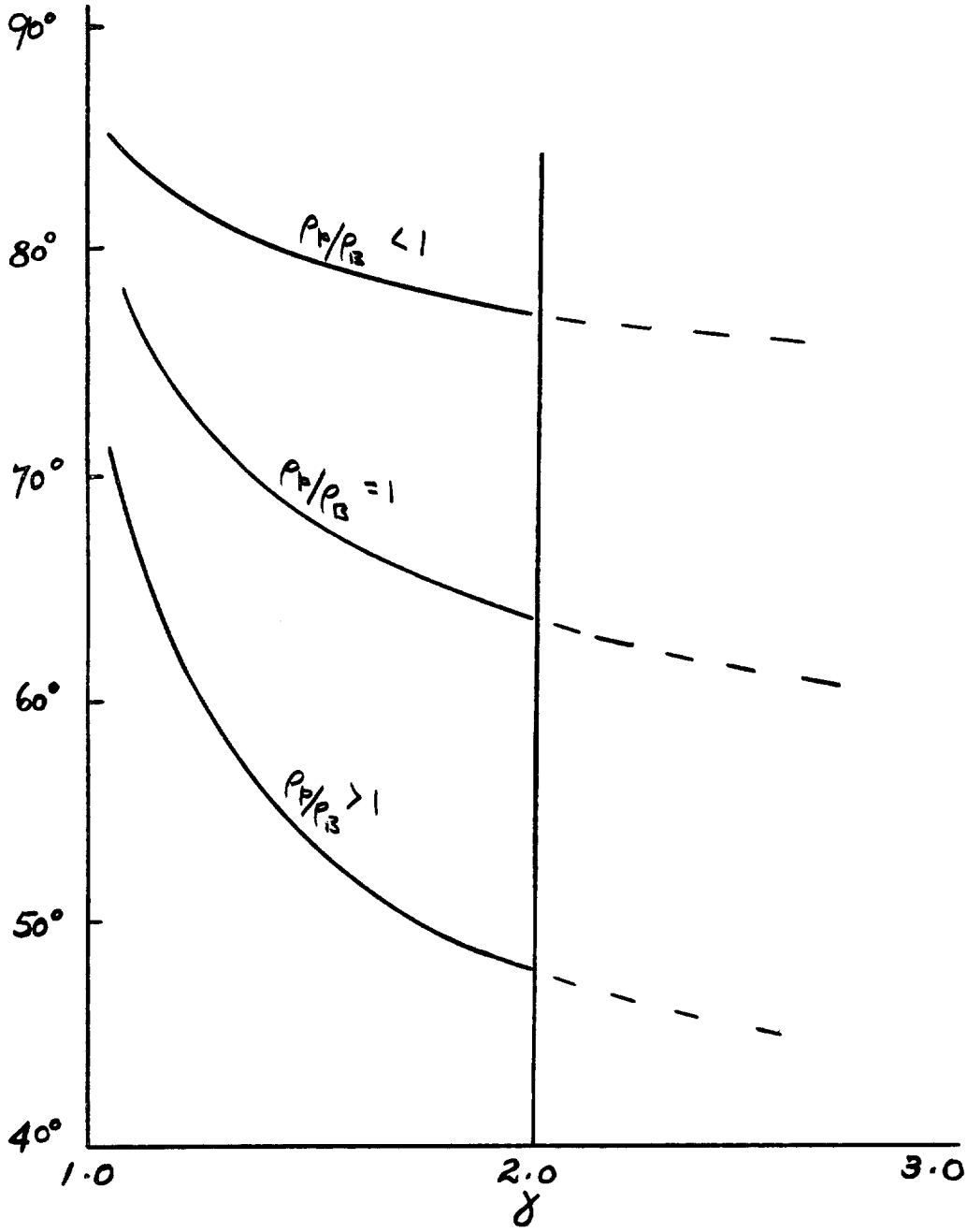

FIG 4.2.2

pressure and density, the others moving less rapidly and with finite pressure and temperature. Since the jet is in vacuum, a cylindrical release wave is formed which moves inward, interacting with the axial wave and spreading the jet radially, although with a lower escape velocity than the axial wave since the action of the latter has reduced the sound speed in the jet where it issues from the cavity to a fixed value of $\frac{2}{\gamma+1} \cdot a_o$.

Inside the converging radial (cylindrical) rarefaction, the flow is one-dimensional and the velocities and states can be calculated analytically since the wave is centered. No attempt has been made to calculated the interaction field flow analytically, but a numerical solution of the flow equations in finite difference form has given a fairly accurate picture of the conditions existing in this region. The inner and outer boundaries of the interaction field can be derived analytically and their location is calculated with fair agreement by the numerical solution. Typical flow patterns and energy and momentum distributions are shown in section 7.1 figures (7.1.8 to 7.1.12).

It should be realized that the flow conditions are short term only, in that the shocked state is considered as constant with time (although otherwise the flow is very

"unsteady"). The validity of the model breaks down when the pellet shock decays significantly due to interaction with the rarefaction, or when the pellet trailing face reaches the pellet shock and the latter reflects as a right-moving rarefaction. Since the former occurs in the time it takes the shock to travel only a few bumper thicknesses, the illustrated flow pattern applies for distances of the order of one or two pellet diameters downstream of the bumper. Nevertheless, the model is essential to show the initial stage of the expansion flow, which governs its long term expansion, as described in section 4.4.

For some combinations of γ and σ, (for example, $\gamma > 3$, $\sigma = 1$), the pellet shock moves upstream of the bumper and a cylindrical release wave forms and propagates into the shocked material behind the shock, figure 10. As will appear in the next section however, the time during which this takes place is limited by the deceleration of the shock when the axial rarefaction overtakes it, and it is swept back into the bumper by the unshocked pellet. Consequently its main significance appears at present to be as a possible experimental indicator of the effective value of γ, since this wave will splash pellet material onto the front face of the bumper.

4.3 Rarefaction, Interaction and Shock Decay

For any value of δ and σ the axial rarefaction wave, initiated when the bumper shock reaches the downstream side of the bumper, will overtake the pellet shock and decay its strength. The time taken for this to occur will depend on δ and σ.

Figure 4.3.1 illustrates the standard numerical processes (refs. 9, 10) for the rarefaction wave interaction and shock decay in the x-t plane. The entropy change behind the decaying shock and across reflected interfaces were neglected. The sound speed in the unshocked material was assumed to be zero as was done in reference 1.

Figures 7.2.3 to 7.2.6 show the post-shock pressures as a function of the shock location in the pellet from the original leading edge of the pellet for various values of δ and σ. The shaded areas indicate where the shock is enclosed within the bumper.

Since the shock decay is accompanied by shock deceleration the shock will eventually be swept downstream of the bumper in all cases. For certain values of δ and σ the shock may initially progress upstream of the bumper. Whenever the shock progresses outside the bumper radial rarefaction waves will be initiated and tend to decay the shock strength.

SHOCK RAREFACTION INTERACTION

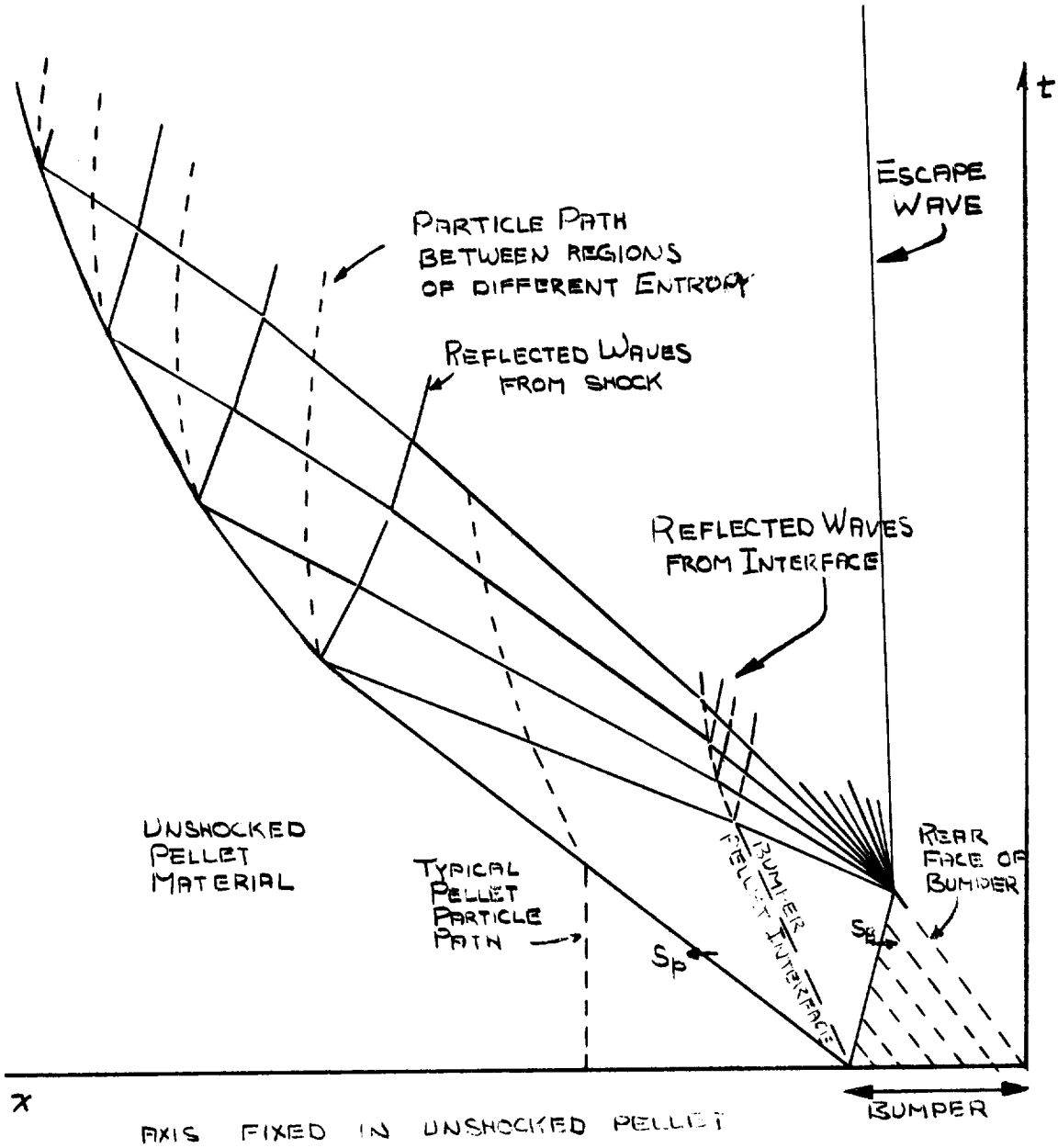

FIG. 4.2.1

The time taken for the radial rarefaction wave to reach the centre of the pellet was calculated as a function of D/δ for various values of γ and σ, figures 7.2.8 and 7.2.10. This was done allowing for the axial decay of the shock.

A stepwise numerical process is being carried out at present to determine the decay of the shock strength due to the radial rarefaction waves only.

Figure 3.1 was obtained from the results of the axial decay analyses and show the critical pellet length to thickness as a function of impact pressure for $\gamma = 3$ and values of σ.

4.4 Long Term Expansion Process

The expansion of the gas cloud after the pellet has been shocked and only expansion waves exist (assuming expansion into a vacuum) is very complex. The shocked states are non-uniform due to shock decay and the shocked particles are released at non-uniform time rates. The velocity and density distribution of the gas cloud will depend on the length/diameter ratio of the pellet and the bumper thickness/pellet diameter ratio, even for similar bumper and pellet materials.

A crude first approximation for the long term expansion of the gas cloud was set up, considering the gas cloud to be formed by the expansion of a sphere of compressed gas into a vacuum. This approximation was used to predict the stagnation pressure the vehicle skin would receive at various spacings from the bumper plate (figures 7.3.9 and 7.3.10).

In order to match as closely as possible the short time expansion characteristics it was necessary to translate the sphere as it expanded. The translational velocity was taken as that of the shocked material which will only be true for the centre of mass of the sphere if the bumper material punched out has the same mass as the pellet. However, the initial expansion was carried out as though this were the case. The effect of a thin bumper would require a small modification of the subsequent expansion as a result of pellet shock decay.

The radial expansion velocity was taken as the radial escape velocity associated with the cylindrical release wave acting on the gas jet described in section 4.1. This value is $(\frac{2}{\gamma+1})$ times the axial escape velocity and thus the gas cloud expands as an ellipsoid rather than a sphere. Although this distortion is now being handled analytically, it was decided to interpolate between the

results of spherical expansion at axial escape velocity and spherical expansion at radial escape velocity as a first approximation.

5.0 FURTHER THEORETICAL CONSIDERATIONS

Shock Decay

The shock wave decay due to an edge rarefaction is now being analysed by a step by step graphical method as no standard analytical approach to such an interaction could be found. The combination of the axial and radial rarefaction interactions and their result on the decay of the shock strength should be combined to give the total shock decay. No reasonable simple solution to this problem has been found so far.

Gas Cloud Expansion

The one-dimensional region of the initial expansion system both analytical and numerical could be expanded to allow for the shock strength decay. In the two-dimensional region the numerical computer solution is now giving reasonably accurate results for the short time velocity and density distribution. This program also could be expanded to allow for the shock strength decay.

The solution of the long term expansion process which was handled analytically by approximate methods based on the expanding sphere, could be programmed using the basic flow equation as it would be a self similar solution of an ellipsoid. Such a solution, although subject to errors due to the finite difference approximation, would

satisfy all three conservation laws and thus be an improvement over the simple analytical solution. In addition, by substituting the conditions calculated by the two dimensional method at the time the end of the pellet reaches the shock for the uniform sphere as initial conditions, a better approximation to the physical case could be obtained. Finally, the effect of radiation, assuming transparent material, could be introduced into the energy equation.

Ionization

The use of the perfect gas equation of state to evaluate the temperature of the compressed material is probably the most significant approximation thermodynamically. The shock process will transmit energy by molecular collision and in the process will rupture the inter-crystalline bonds; after a few collisions the molecular motion will be random. Dissociation of polyatomic molecules will occur next, followed by ionization, both processes reducing the temperature of the shocked state and altering the value of the gas constant. Not only does ionization alter the temperature behind the shock, but the strong-shock density relation used in the analysis is in serious error as shown in reference 8, for strong shock in argon.

Effect of Finite Bumper Thickness

The reduction in pellet shock strength and the effect on the subsequent flow of a two dimensional bumper shock should be analysed.

The effect of shapes other than cylinders needs to be considered. A cone would appear to be the next shape in order of complexity, since it is still axi-symmetrical. It is, in addition, one of the most effective penetrators, so that it's study could well be rewarding. Qualitatively extrapolating the effects which appear from the analysis of the cylinder, the core would seem to tend to retain a point as a result of decay of the shock system, particularly for $\gamma < 3$, as outlined schematically in figure 5.1. The centre of the pellet shock would decay more rapidly than the edges and a pointed pellet would be the end product of the shock system.

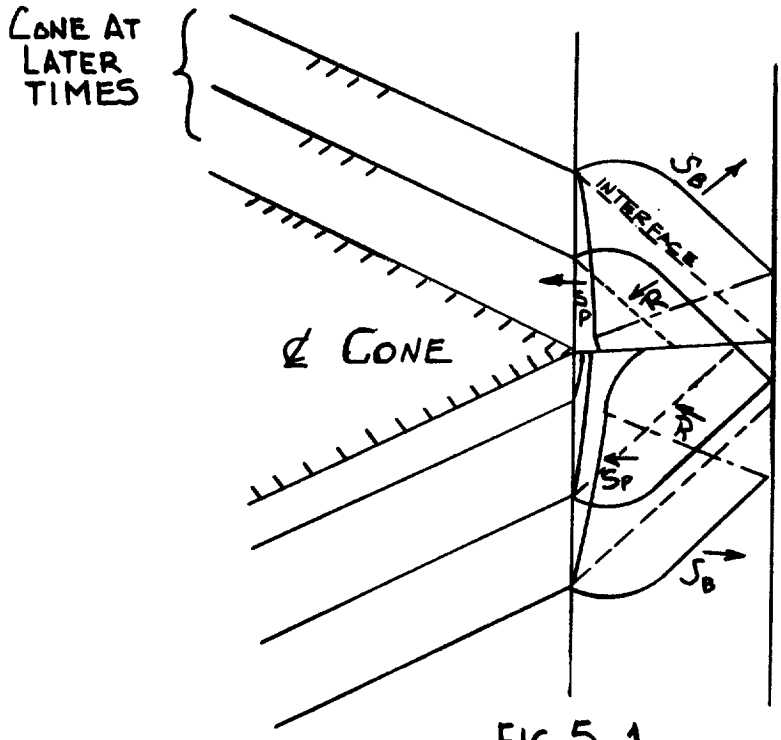

FIG. 5.1

(TOP & BOTTOM HALVES SHOW PATTERN AT ALTERNATING TIMES AFTER IMPACT COMMENCES)

6.0 EXPERIMENTAL PROGRAM

The experimental program can be directed in a number of ways, as follows:

1) Physical studies of shocked media to determine equations of state and flow characteristics of such media.
2) Verification of fluid dynamic analysis with shock tubes simulating the models.
3) Impact tests to determine similarity between model and actual impact, to establish suitable values for γ , and to determine the effects of radiation, ionization, etc.

Any one of these programs will require considerable time, staff, and equipment, it will therefore be necessary to study those most likely to provide corroboration of the theory and fruitful results as a basis for further analysis.

Impact tests are already underway, and by suitable choice of materials reasonable simulation of meteoroid impact states should be achievable. It would appear that arsenic, cesium, chromium, iodine, potassium and sulphur would be suitable materials, all having low total heats of vapourization.

Using such materials, tests will be carried out at velocities of 8 km/sec and higher. Flash x-ray, ion detectors and splash examination will be used to

measure spray angle and distribution, which in turn will help evaluate γ . Quartz crystal pressure gauges, thin film thermocouples and ballistic pendulum techniques on the witness plate will be used to measure momentum and energy distribution and pressure in the gas cloud as a function of spacing.

Shock tube studies which in effect duplicate the models analysed could be carried out within the state of the art. Such studies could investigate the expansion characteristics of a variety of substance, including water, which would be expected to undergo a rapid change in γ as it flashes into vapour. It could also be used to study the edge decay of a shock by a cylindrical rarefaction, and the spray angle resulting from the release behind a travelling strong shock.

7.0 DETAILED ANALYSIS

7.1 Initial Expansion

The analysis of the initial expansion flow assumes the shocked states as defined by equations 14 through 22 of reference 1. The decay of the pellet shock strength is neglected and the time of the initial expansion analyses is limited to the time before the pellet shock reaches the end of the pellet. With these assumptions and limitations the initial expansion analysis can be carried out assuming a constant shocked state of bumper and pellet (σ assumed equal to 1) material is being fed into the expansion of the gas into a vacuum. The head of the radial rarefaction wave was assumed to move radially into the one-dimensional axial flow at the local acoustic velocity, and swept downstream in an axial direction at the local particle kinetic velocity. However, the head of the radial rarefaction wave will in fact always move normal to its own boundary. The assumption that its movement is purely radial simplifies the analysis for this first approximation.

Figures 7.1.1 and 7.1.2 show in the (xy) and (xt) planes respectively, the assumed conditions existing in the shocked states prior to the initiation of the expansion process.

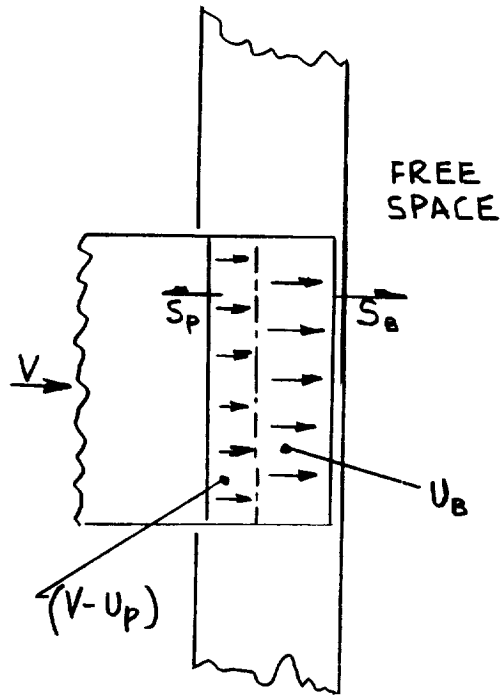

FIG 7.1.1

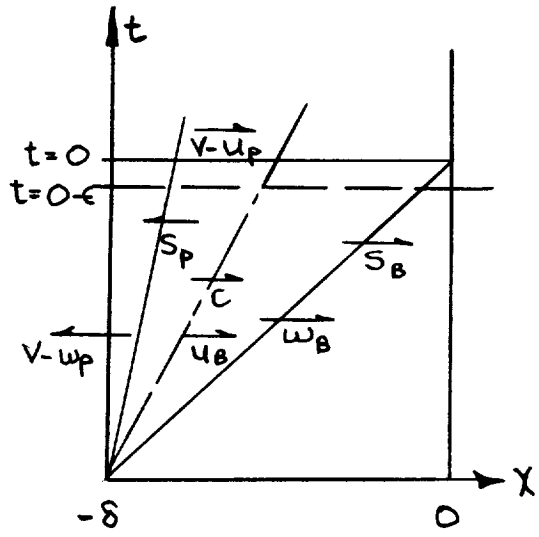

FIG 7.1.2

IMPACT CONDITIONS JUST PRIOR TO THE FORMATION OF $\overleftarrow{R_A}$

The conditions after the formation of $\overleftarrow{R_A}$ are illustrated in Figures 7.1.3 and 7.1.4 .

Within the one-dimensional region of the expansion process, the following relations govern the flow.

1) The slope of any C characteristic is given by

$$\frac{x}{t} = u - a, \qquad 7.1.1$$

and 2) for any particular particle, $u + \frac{2}{\gamma - 1}.a$ must always remain constant, thus

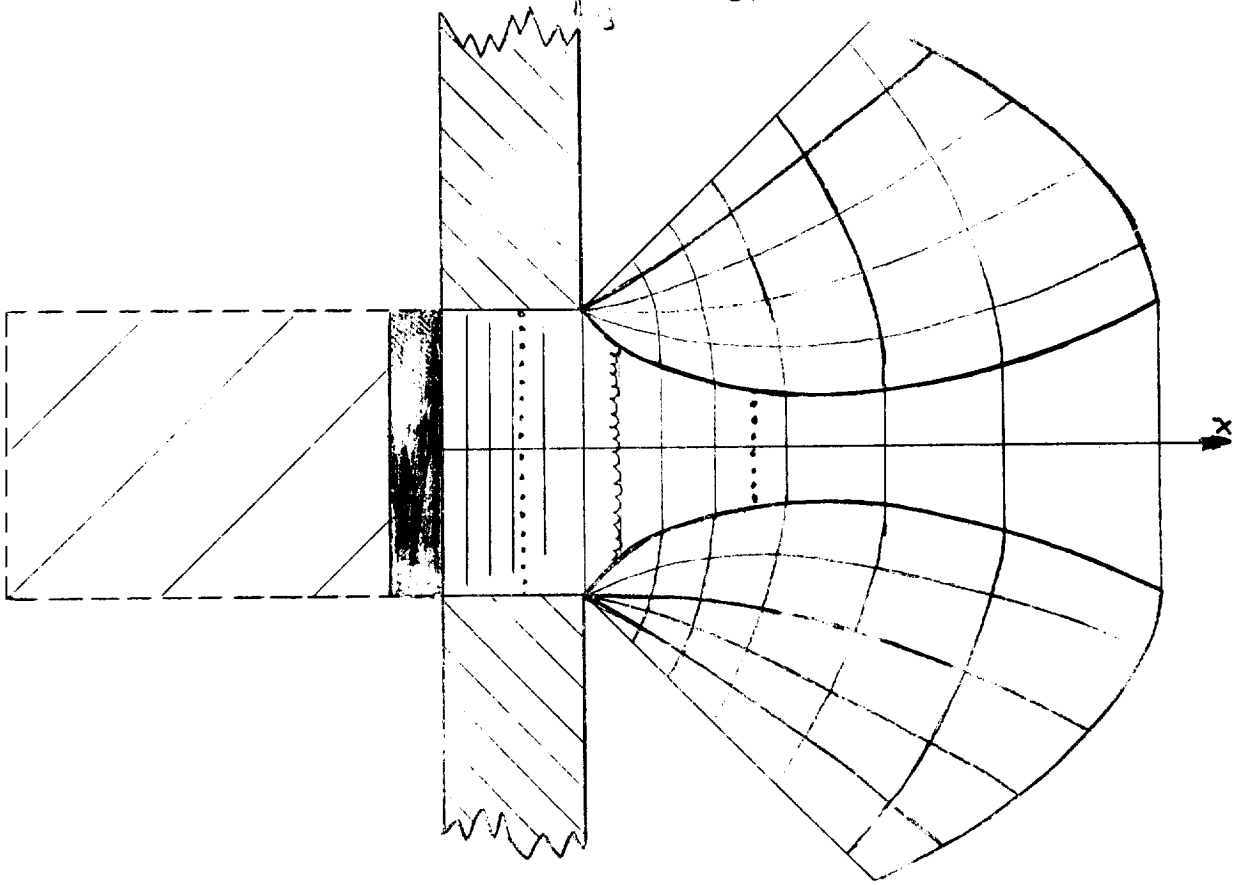

x, y plane

Fig 7.1.3

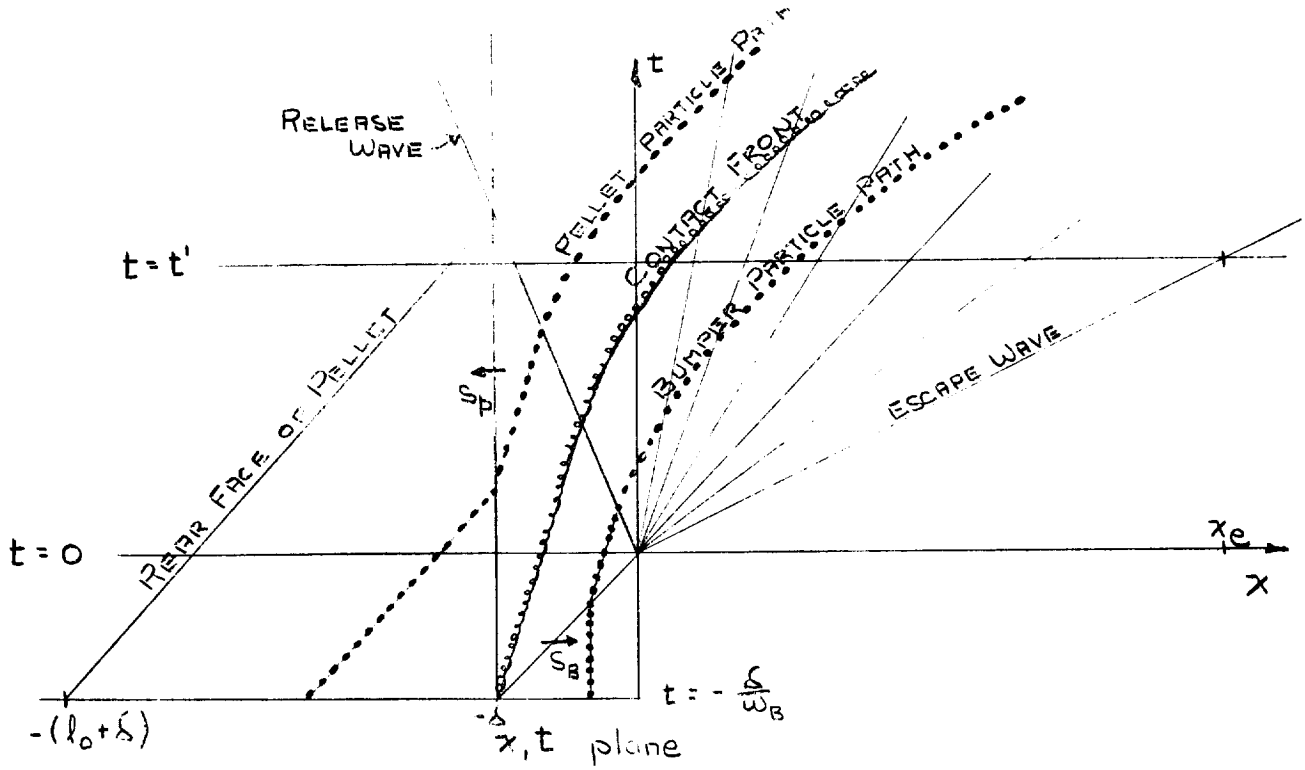

FLOW AFTER FORMATION OF $\overleftarrow{R}_B$

Fig 7.1.4

$$u + \frac{2}{\gamma-1}\cdot a = u_o + \frac{2}{\gamma-1}\cdot a_o \qquad 7.1.2$$

Combining and rearranging these equations in a manner similar to that of Ref. 9 yields

$$u = \frac{2a_o}{\gamma+1} + \frac{\gamma-1}{\gamma+1}\, u_o + \frac{2}{\gamma+1}\,\frac{x}{t} \quad , \qquad 7.1.3$$

and $$a = \frac{2a_o}{\gamma+1} + \frac{\gamma-1}{\gamma+1}\, u_o - \frac{\gamma-1}{\gamma+1}\,\frac{x}{t} \qquad 7.1.4$$

Since $u = \frac{dx}{dt}$ = local particle velocity

$$\frac{dx}{dt} - \frac{2}{\gamma+1}\,\frac{x}{t} = \frac{2a_o}{\gamma+1} + \frac{\gamma-1}{\gamma+1}\, u_o \cdot \qquad 7.1.5$$

The standard solution for equations of this type yields

$$x = (u_o + \frac{2a_o}{\gamma-1})\, t + Kt^{\frac{2}{\gamma+1}} \cdot \qquad 7.1.6$$

Equation 7.1.6 gives the general solution for the axial displacement of the bumper particles downstream of the rear face of the bumper; for the particular solution for the particle distribution at a specific time after impact, the arbitrary constant K is evaluated with reference to Figure 7.1.5.

The head of the rarefaction $\overleftarrow{R_A}$ sweeps into the shocked bumper material with velocity $(a_o - u_o)$, where a_o is the local sound speed, and u_o is the translational velocity of the shocked bumper state.

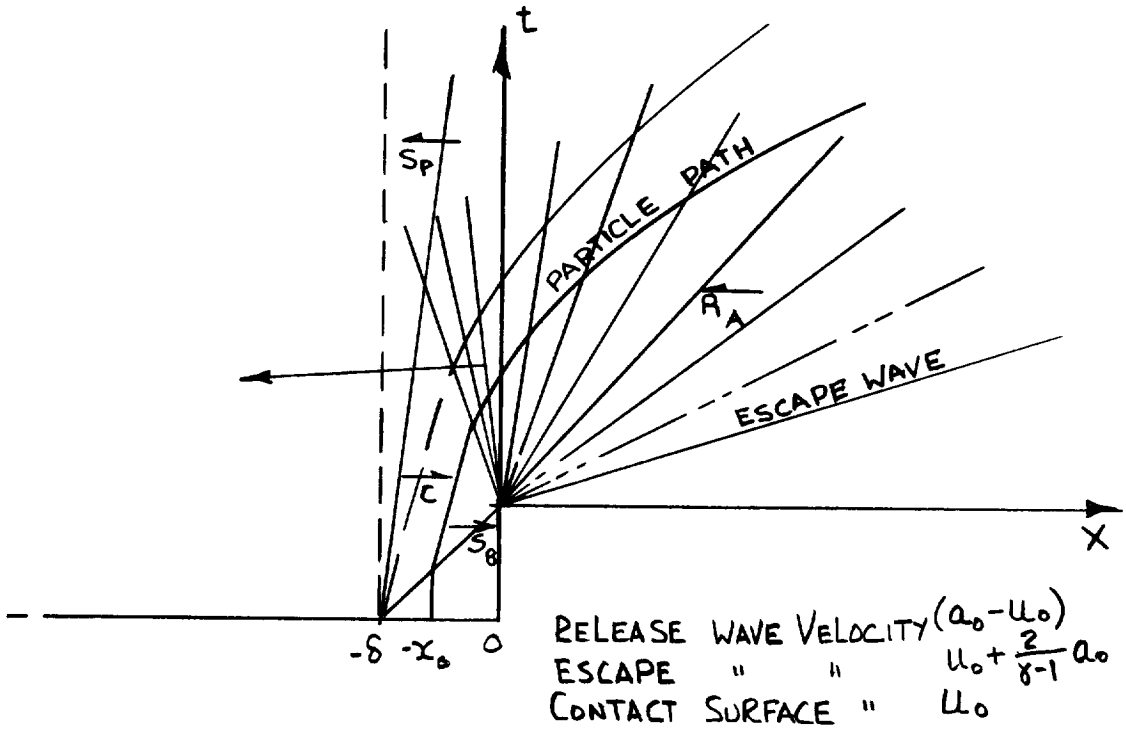

PATH OF SPECIFIC BUMPER PARTICLE

FIG 7.1.5

Since all of the shocked bumper material is travelling at the velocity u_o at time t=o (note that here t=o is taken as the time at which $\overleftarrow{R_A}$ is formed), an initial position within the shocked state may be defined by $x = u_o t_o$, where t_o varies from 0 at the rear face of the bumper to $(-\frac{\delta}{w_B})$ at the contact region separating the pellet and bumper particles. The constant in equation 7.1.6 is evaluated for the general particle initially at $x = -x_o$, where $-\delta < -x_o < 0$, by computing its value at the position $x = (u_o - a_o)t$, $t = t_o$

Thus
$$K = -\left(\frac{\gamma+1}{\gamma-1}\right) a_o t_o^{\frac{\gamma-1}{\gamma+1}} \qquad 7.1.7$$

and
$$x = \left(u_o + \frac{2a_o}{\gamma-1}\right) t - \left(\frac{\gamma+1}{\gamma-1}\right) a_o t_o \left(\frac{t_o}{t}\right)^{-\frac{2}{\gamma+1}} \qquad 7.1.8$$

Combining 7.1.8 with 7.1.2 and 7.1.3 yields
$$u = u_o + \frac{2}{\gamma-1} a_o - \frac{2}{\gamma-1} a_o \left(\frac{t_o}{t}\right)^{\frac{\gamma-1}{\gamma+1}} \qquad 7.1.9$$

$$a = a_o \left(\frac{t_o}{t}\right)^{\frac{\gamma-1}{\gamma+1}} \qquad 7.1.10$$

The centred cylindrical rarefaction $\sqrt{R_C}$ accelerates peripheral shocked particles from the bumper to the radial escape velocity as soon as they emerge from the exit plane, excepting those particles accelerated to the axial escape velocity by $\overleftarrow{R_A}$. The head of $\sqrt{R_C}$ sweeps radially into the one dimensional flow regime of $\overleftarrow{R_A}$ at the local sound speed and is itself swept axially at the local particle velocity. (The cylindrical rarefaction does not in fact sweep into the one dimensional axial expansion purely radially, but in a direction normal to its head. The assumption of radial motion greatly simplifies the analysis although it introduces some error in the wave shape, particularly near the escape boundary and the bumper orifice). The inward progression of $\sqrt{R_C}$ is given by

$$y = y_o - \int a\,dt + K \qquad 7.1.11$$

which on substitution from equation 7.1.10 and integration yields

$$y = y_o - \frac{\gamma+1}{2} a_o t \left(\frac{t_o}{t}\right)^{\frac{\gamma-1}{\gamma+1}} + K \,. \qquad 7.1.12$$

$\sqrt{R_C}$ originates the instant any particles emerge from the exit plane; its influence is therefore felt by the plane of particles originally at a position defined by $x = -x_o$ at $t = -\frac{\delta}{w_B}$ (see figure 7.1.5), when sufficient time has elapsed for this plane of particles to reach the exit plane. This time,

$$t = t' = t_o \left(\frac{\gamma-1}{\gamma+1}\frac{u_o}{a_o} + \frac{2}{\gamma+1}\right)^{-\frac{\gamma+1}{\gamma-1}} \qquad 7.1.13$$

is found by setting x=o in equation 7.1.8. The constant K in 7.1.12 is then evaluated by using the condition that at this value of t, $y = y_o$, with the result

$$K = \frac{\gamma+1}{2} a_o t_o \left(\frac{\gamma-1}{\gamma+1}\frac{u_o}{a_o} + \frac{2}{\gamma+1}\right)^{-\frac{2}{\gamma-1}} \qquad 7.1.14$$

Thus

$$y = y_o + \frac{\gamma+1}{2} a_o t_o \left(\frac{\gamma-1}{\gamma+1}\frac{u_o}{a_o} + \frac{2}{\gamma+1}\right)^{-\frac{2}{\gamma-1}} - \frac{\gamma+1}{2} a_o t \left(\frac{t_o}{t}\right)^{\frac{\gamma-1}{\gamma+1}} \qquad 7.1.15$$

This expression used in conjunction with 7.1.8 defines, for any value of t (i.e. elapsed time), and a range of applicable values of t_o, the boundary separating the axial and radial flow regimes.

End of Bumper Flow

The pure bumper flow ceases when the contact surface $\vec{C}$ reaches the exit plane x=o. The time required for this to occur is obtained by setting x=o in equation 7.1.8 and inserting the appropriate value of t_o.

The position of the plane of particles in the front face of the bumper at time of impact ($t=t_i$) is $x = -\delta$. The position at t=o is $(-\delta + u_B.\frac{\delta}{w_B})$

i.e. $$\frac{x}{t-o} = \delta\,(\frac{u_B}{w_B} - 1) \qquad 7.1.16$$

From equation 16, reference 1, $\frac{u_B}{w_B} = \frac{2}{\gamma_B + 1}$, thus

$$\frac{x}{t=o} = -\,(\frac{\gamma_B - 1}{\gamma_B + 1}) \qquad 7.1.17$$

The point of intersection of $\vec{C}$ and the head of $\overleftarrow{R_A}$ is, from figure 7.1.5

$$x = \frac{\gamma_B - 1}{\gamma_B + 1}\,(\frac{u_B}{a_B} - 1), \quad t = \frac{\gamma - 1}{\gamma + 1}\,\frac{\delta}{a_B} \qquad 7.1.18$$

or, using equation 15 and 20 from reference 1 and the definition of σ

$$x = \sqrt{\frac{2}{\gamma(\gamma-1)} - 1}\,\frac{\gamma-1}{\gamma+1}.\delta, \quad t = \sqrt{\frac{2}{\gamma(\gamma-1)}}.(\sigma+1)\,\frac{\delta}{v} \qquad 7.1.19$$

Equation 7.1.8 becomes

$$x = 0 = (u_o + \frac{2a_o}{\gamma-1})\, t - (\frac{\gamma+1}{\gamma-1})\, a_o t_o\, (\frac{t_o}{t})^{-\frac{2}{\gamma+1}} \qquad 7.1.20$$

where $t_o = \frac{\gamma-1}{\gamma+1}\frac{\delta}{a_B}$

thus $$t = (\frac{\gamma-1}{\gamma+1}\frac{u_o}{a_o} + \frac{2}{\gamma+1})^{\frac{\gamma-1}{\gamma+1}} \cdot (\frac{\gamma-1}{\gamma+1}\frac{\delta}{a_o}) \qquad 7.1.21$$

or $$t = \frac{\delta}{V} \cdot (\frac{\sigma+1}{\gamma-1})\sqrt{\frac{2(\gamma-1)}{\gamma}} \cdot \left[\frac{2}{\gamma+1}\left(\sqrt{\frac{\gamma-1}{2\gamma}} + 1\right)^{\frac{\gamma-1}{\gamma+1}}\right] \qquad 7.1.22$$

Equation 7.1.22 is plotted in figure 7.1.6.

Momentum and Energy Density and Flux

The momentum density per unit volume of the gas cloud downstream of the bumper plate is given by:

$$M = \rho u \qquad 7.1.23$$

where ρ and u refer to local conditions.

The distribution of particle velocity u throughout the one dimensional axial flow is given by equation 7.1.9.

The density distribution is calculated assuming isentropic expansion in the one dimensional axial rarefaction wave, viz. from

$$p = A\rho^{\gamma} \qquad 7.1.24$$

$$\frac{\rho}{\rho_o} = (\frac{a}{a_o})^{\frac{2}{\gamma-1}} \qquad 7.1.25$$

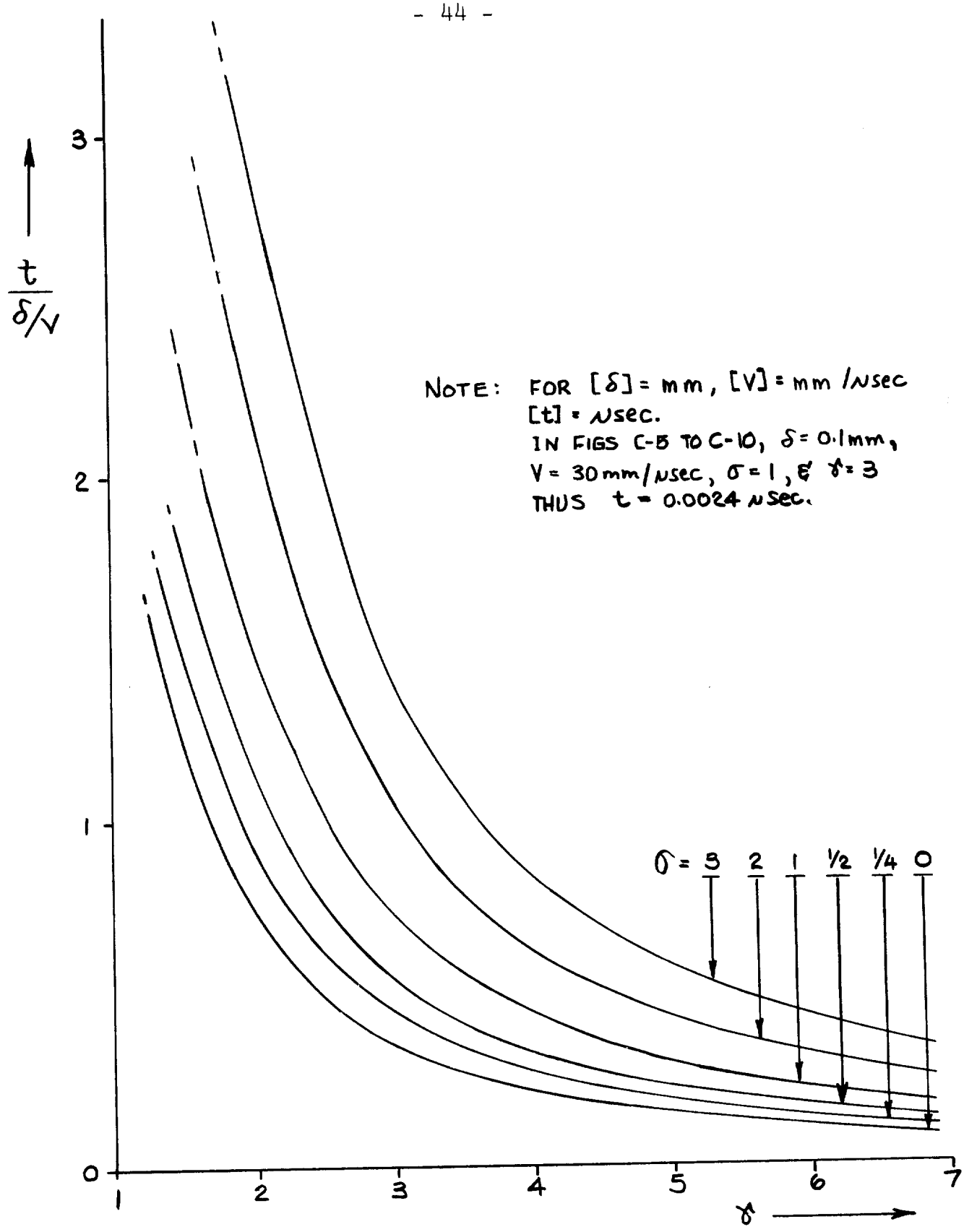

GRAPH OF EQUATION 7.1.22

FIG 7.1.6

Also $$\rho_o = \frac{\gamma p_o}{a^2_o} \qquad 7.1.26$$

$$p_o = \frac{\gamma+1}{2} \rho_{B_o} \frac{\sigma^2 V^2}{(1+\sigma)^2} \quad \text{(equation 17, ref. 1)} \qquad 7.1.27$$

i.e. $$\rho_o = \frac{\gamma}{a_o^2} \cdot \frac{\gamma+1}{2} \cdot \left(\frac{\sigma V}{1+\sigma}\right)^2 \cdot \rho_{B_o} \qquad 7.1.28$$

and $$\rho = \frac{\gamma+1}{2} \left(\frac{\sigma V}{1+\sigma}\right)^2 \cdot \frac{\gamma \rho B_o}{a_o^2} \cdot \left(\frac{a}{a_o}\right)^{\frac{2}{\gamma-1}} \qquad 7.1.29$$

Thus M is computed by combining 7.1.9 and 7.1.29. The momentum flux M_f is defined by

$$M_f = Mu = \rho u^2 \qquad 7.1.30$$

and is obtained by combining $(7.1.9)^2$ and 7.1.29. The significance of the momentum flux is seen on noting that the pressure force exerted by the gas cloud on the witness plate, or vehicle hull, is the result of the reaction of the hull in producing a change in the momentum of the gas cloud particles.

The energy density per unit volume is given by the sum of the local particle kinetic energy and the local residual thermodynamic energy, viz.

$$E = \rho \left(\frac{1}{2} u^2 + C_v T\right) \qquad 7.1.31$$

The kinetic energy term is similar to (7.1.30); the thermodynamic energy is found by noting that

$$\rho c_v T = \frac{\rho a^2}{\gamma(\gamma-1)} \quad . \qquad 7.1.32$$

Thus $$E = \frac{1}{2}\rho u^2 + \frac{\rho a^2}{\gamma(\gamma-1)} \quad , \qquad 7.1.33$$

where the latter term is evaluation by substitution of equations 7.1.10 and 7.1.29 in 7.1.33.

The energy flux E_f is defined by

$$E_f = E.u = \frac{1}{2}\rho u^3 + \frac{\rho a^2 u}{\gamma(\gamma-1)} \quad , \qquad 7.1.34$$

where equations 7.1.9, 7.1.10 and 7.1.29 are used in evaluating 7.1.34.

Equations 7.1.23, 30, 21 and 34 are plotted in figure 7.1.8 as a function of displacement with the gas cloud. In figures 7.1.9, 10, 11 and 12 an attempt has been made to show the approximate relative distributions of M, M_f, E and E_f through theone dimensional axial flow, and also in the mixed radial and axial flow regime. The distributions of M, M_f, E and E_f in the two dimensional region outside the central one dimensional core were approximated assuming the total density increase outside the original cylindrical boundary was equal to the decrease inside the original cylindrical boundary.

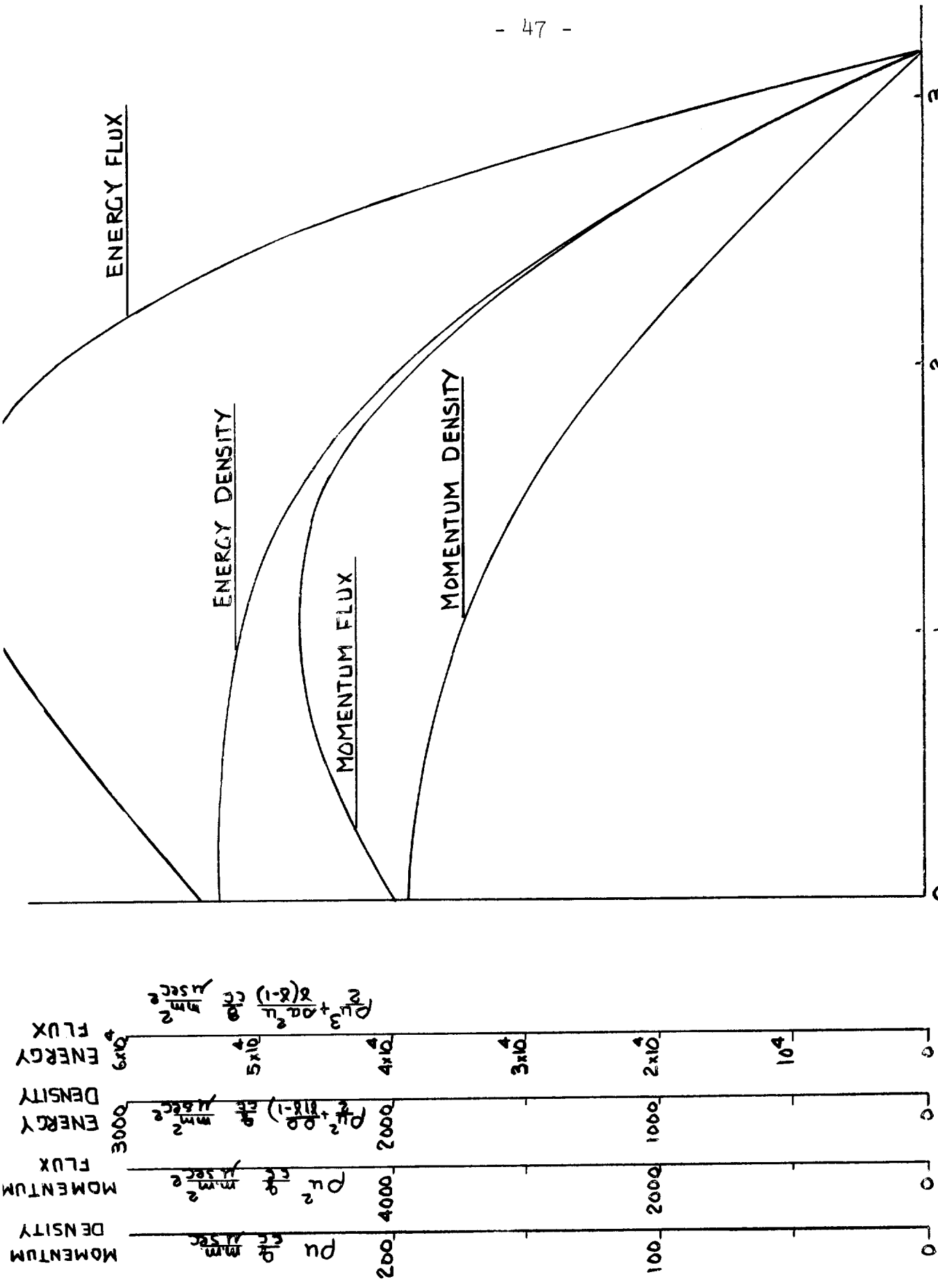

FLOW PARAMETERS IN ONE-DIMENSIONAL INITIAL EXPANSION

FIG 7.1.8

MOMENTUM DENSITY DISTRIBUTION IN EXPANSION CLOUD

(RELATIVE TO UNIT EXIT PLANE DISTRIBUTION)

$\gamma_p = \gamma_B = 3$, $V = 30$ mm/μsec, $y_o = 1$ mm, $\ell_o = 2$ mm, $\delta = 0.1$ mm, $t = 0.077$ μsec, $\rho_{Bo} = \rho_{po}$

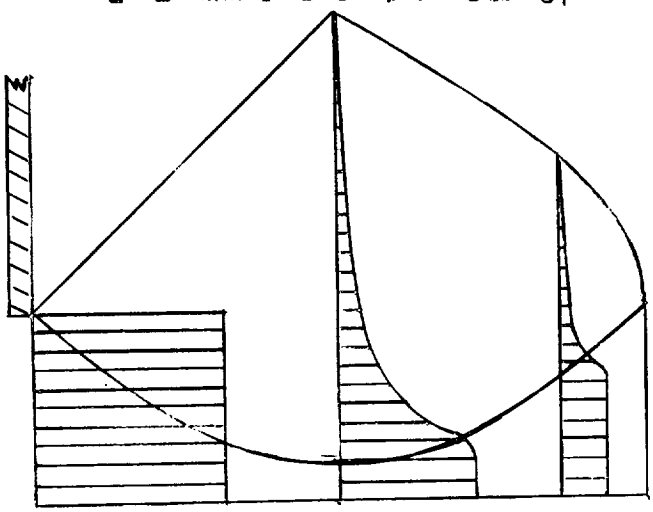

FIG 7.1.9

MOMENTUM FLUX DISTRIBUTION IN EXPANSION CLOUD

(RELATIVE TO UNIT EXIT PLANE DISTRIBUTION)

$\gamma_p = \gamma_B = 3$, $V = 30$ mm/μsec, $y_o = 1$ mm, $\ell_o = 2$ mm, $\delta = 0.1$ mm, $t = 0.077$ μsec, $\rho_{Bo} = \rho_{po}$

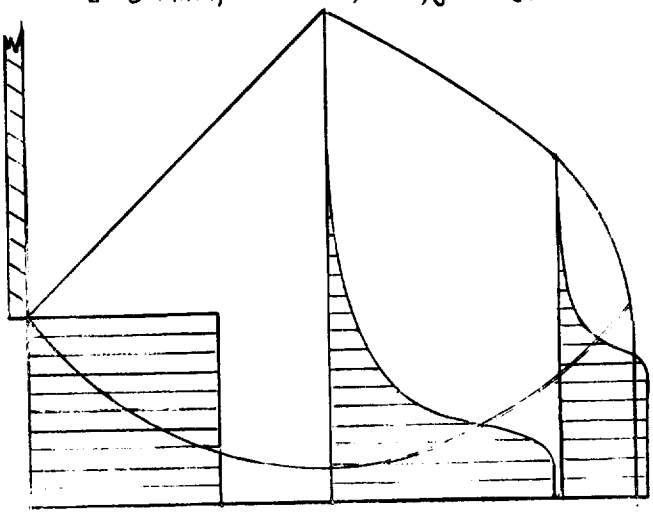

FIG 7.1.10

ENERGY DENSITY DISTRIBUTION IN EXPANSION CLOUD

(RELATIVE TO UNIT PLANE DISTRIBUTION)

$\gamma_p = \gamma_s = 3$, $V = 30$ mm/μsec, $y = 1$ mm, $\ell_o = 2$ mm, $\delta = 0.1$ mm, $t = 0.077$ μsec $\rho_{Bo} = \rho_{po}$

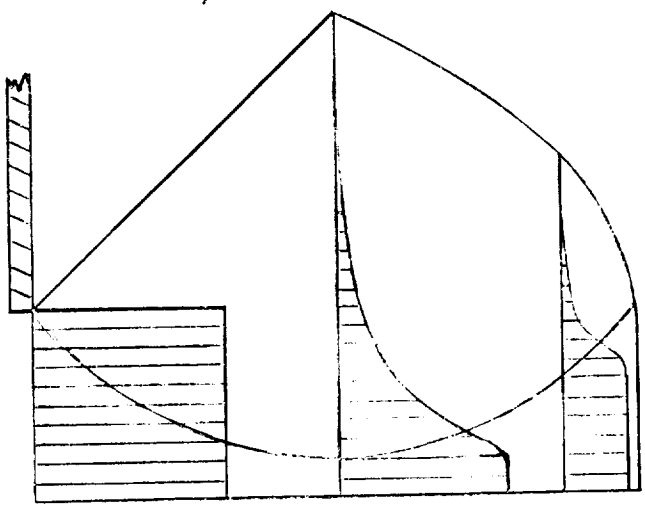

FIG 7.1.11

ENERGY FLUX DISTRIBUTION IN EXPANSION CLOUD

(RELATIVE TO UNIT EXIT PLANE DISTRIBUTION)

$\gamma_p = \gamma_s = 3$, $V = 30$ mm/μsec, $y = 1$ mm, $\ell_o = 2$ mm, $\delta = 0.1$ mm, $t = 0.077$ μsec, $\rho_{Bo} = \rho_{po}$.

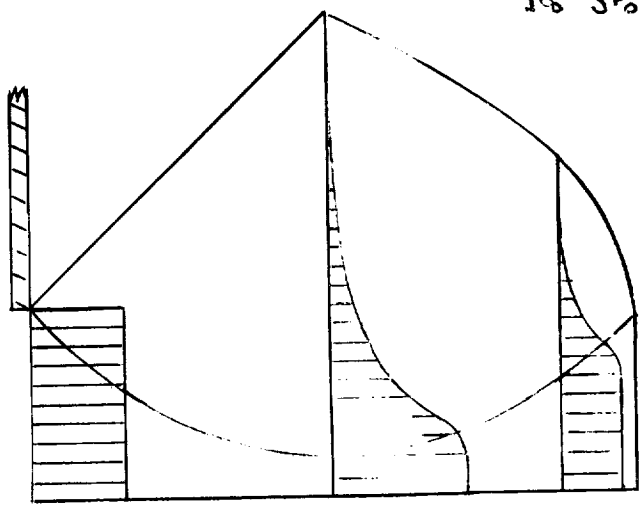

FIG 7.1.12

The momentum density represents the impulse acting on a surface when struck by unit volume of the gas, and the momentum flux gives the dynamic pressure at any instant. The pressure, though very large, acts for a very short time, and the dynamic resistance of a material to such brief pressures is not known. The impulse integrated over the duration of the flow, gives the total momentum transferred on to the area of the surface affected.

An interesting modification to the above theory would be to let the shocked state velocity u_o be zero and thus simulate the expansion that would result if a highly energized gas were to suddenly be released from a cavity into a vacuum. The analysis was carried out for this bumper cavity model but not included here because of its similarity to the general theory. It is interesting to note that the free space expansion was found to be bounded by a cone whose semi vertex angle is given by $\theta = \tan^{-1} \frac{2}{\gamma - 1}$. Since this angle depends only on the value of γ, a study of the spray angle should give an indication of the effective polytropic exponent γ.

It is significant that the spray angles predicted by the bumper enclosed model are of the same order as those observed in tests (Ref. 7). Once the

short time flow is cut off by the arrival of the end of the pellet, however, the cone flow angle will remain the same until the flow at exit from the bumper becomes subsonic. Since the radial expansion will take place at the velocity $\frac{2}{\gamma-1} a_{exit}$, but the particle velocity will drop below a_{exit}, the spray angle will increase. However, the density is very low at the periphery of the cloud (of the order of 10^{-10} gm/cm^3) and no measurable splash would be expected outside the angle given by the short time flow model.

A computer analysis of the initial gas expansion was attempted based on the conservation equations applied to a volume of unit area and length equal to the grid spacing along the axis. The velocity and state of the gas was given at the origin and the wave front by the analytical solution previously described in this section.

The rate of inflow of mass, momentum and enthalpy to the control volume was taken as the arithmetic average of the inflow at the beginning and end of the time interval of calculations the properties at the end of the time interval were calculated iteratively until successive values differed by less than 1% throughout the field.

The computer results agreed closely with the analytical results in the one-dimensional region, however, difficulty was found in the two dimensional region outside the central core (i.e. insufficient storage space on the 1410 computer).

It should be remembered that the initial expansions analysis will only apply to distances downstream of about 2 pellet diameters (i.e. before the pellet shock reaches the end of the pellet). It is not likely that this small spacing would be practical for meteor protection, however, this initial expansion analysis could be used to form the initial conditions for a long term expansion analysis.

7.2 Rarefaction, Interactions and Shock Decay

At a time dependent on the bumper thickness, the rarefaction wave reflected at the rear face of the bumper will overtake the pellet shock. Once overtaken, the pellet shock is weakened by the interaction of the rarefaction wave and will slow down so that it is eventually swept downstream through the bumper. Depending on the values of γ and σ the pellet shock may initially progress upstream of the bumper until the axial rarefaction slows it down so that it will re-enter the bumper and

pass out downstream. Whenever the pellet shock is outside the assumed one-dimensional bumper radial rarefaction waves will be initiated as the shocked material expands radially outwards. These radial rarefaction waves will also tend to decay the pellet shock.

In the case of the meteoric impact it has been demonstrated (Ref. 1) that the pellet shock extracts from the meteor kinetic energy considerably more energy than that required to vapourize probable meteoric materials. Eventually the pellet shock will be reduced to an elastic wave due to the interaction with the rarefaction waves. During this interaction the shocked state will gradually be reduced from that of a highly ionized, near Fermi gas state, through lower degrees of ionization, dissociation (where applicable), pulverization (when the energy extracted is less than that required to vapourize, but greater than that required to destroy crystal bonds), "chunking", and finally to that of a shocked but intact solid. Complete breakdown of the usefulness of the Whipple bumper shield occurs if the final two states are reached by a decay process within an impacting meteor.

Decay to the final state in an impacting meteor by the radial rarefaction wave may be particularly serious since the shock decays faster near the periphery

forming, in the limit, when the pellet shock is reduced to an elastic wave, a cup shaped crater in the meteor which, on impacting against a solid wall, (i.e. the vehicle hull) will form a crater similar to that formed by a shaped charge.

The decay of the pellet shock is important as it will fix the thickness and density of the bumper material necessary to vapourize a given pellet impacting at a given velocity. The decay of the pellet shock due to a combination of the axial and radial rarefaction waves is extremely complex mainly due to the interaction of the rarefaction waves with each other in the shocked material. In order to obtain a workable analysis the radial and axial rarefaction waves were considered separately.

7.2.1 Axial Rarefaction Wave

Figure 7.2.1 shows a schematic distance-time diagram of the interaction between the pellet shock and the overtaking centred rarefaction wave. The axis was fixed in the unshocked pellet which was assumed to be to the right of the bumper. This model made the analysis of the interaction simpler by having the waves moving in the positive x direction.

SCHEMATIC x-t DIAGRAM FOR INTERACTION OF PELLET SHOCK AND RAREFACTION WAVE

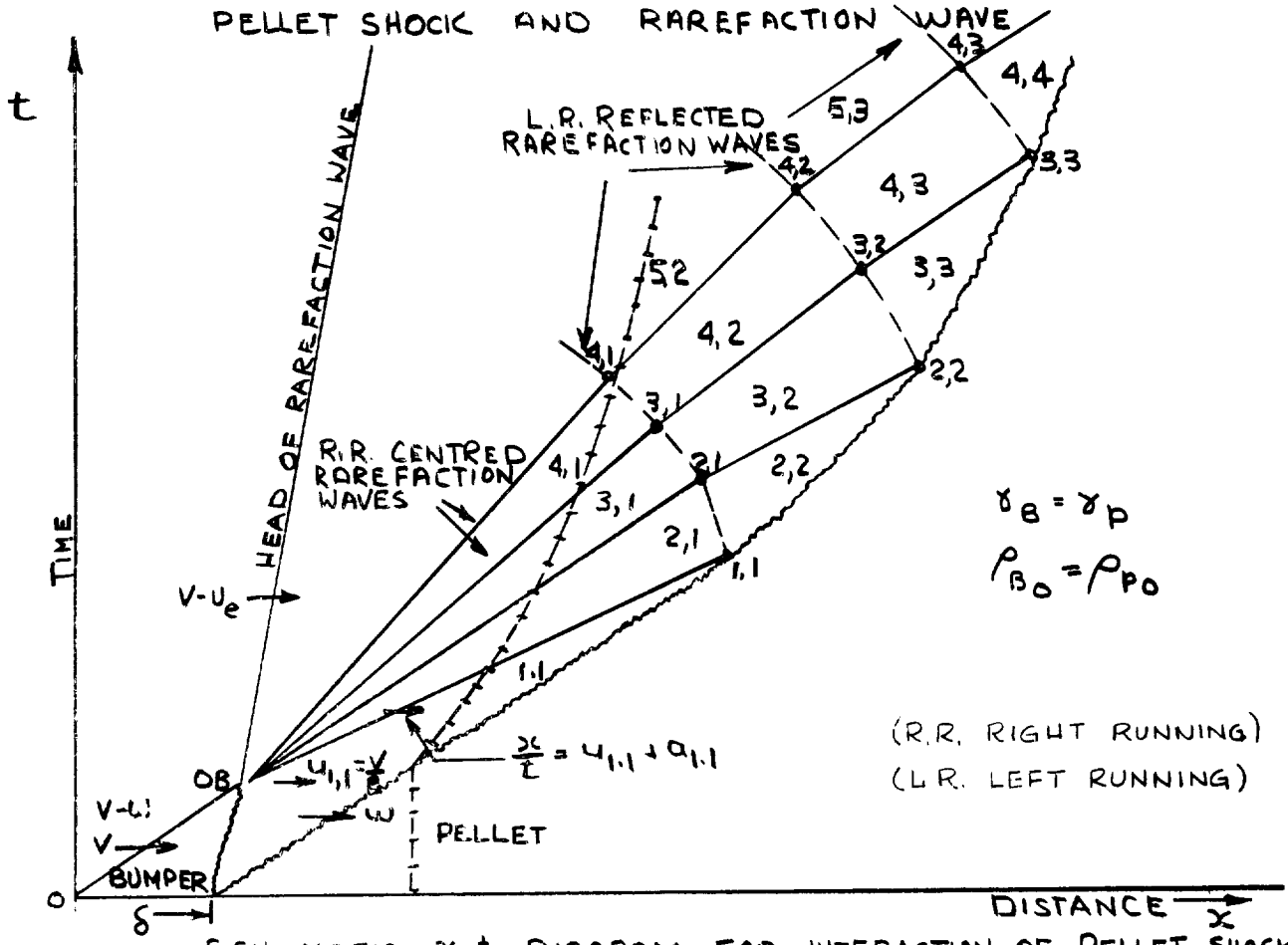

SCHEMATIC x-t DIAGRAM FOR INTERACTION OF PELLET SHOCK AND RAREFACTION WAVE FOR DIFFERENT BUMPER AND PELLET MATERIALS.

FIG 7.2.1

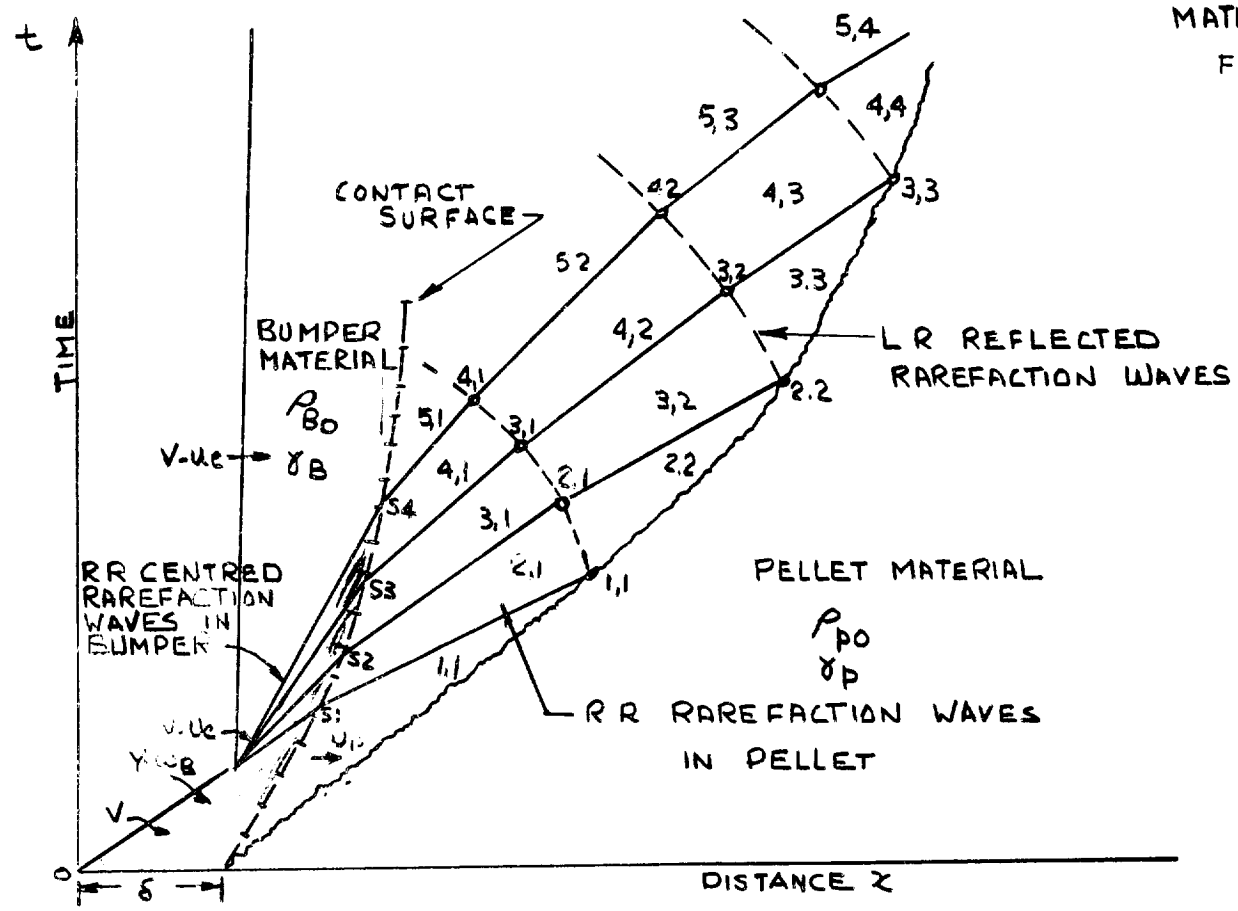

FIG 7.2.2.

It is assumed in the analysis that the entropy was constant over the field considered and therefore the reflected contact surfaces could be neglected and a simple relation between the pressure and the sound velocity obtained. The sound velocity in the unshocked pellet was assumed to be zero and the simple relations across a strong shock with limiting density ratios were used (Ref. 1). The first analysis was done assuming the pellet and bumper had the same density and ratio of specific heats.

The governing equations for the rarefaction waves are:

Across a wave $$u_1 \mp \frac{2}{\gamma-1} a_1 = u_2 \mp \frac{2}{\gamma-1} a_2 \qquad 7.2.1$$

Along a wave $$\frac{x}{t} = u \pm a \qquad 7.2.2$$

The top sign indicates a right-running wave and the bottom sign a left-running wave.

For any regions $$\frac{p_2}{p_1} = \left(\frac{\rho_2}{\rho_1}\right)^{\gamma} = \left(\frac{a_2}{a_1}\right)^{\frac{2\gamma}{\gamma-1}} \qquad 7.2.3$$

Across a shock $$w = \frac{\gamma+1}{2} u_s \qquad 7.2.4$$

$$w = \sqrt{\frac{(\gamma+1)^2}{2\gamma(\gamma-1)}} a_s \qquad 7.2.5$$

For the contact surface between bumper and pellet to maintain separation of the two media,

$$u_{1.1} = \frac{V}{2} \qquad 7.2.6$$

and from 7.2.4 and 7.2.5

$$a_{1.1} = \left(\frac{\gamma}{2\beta}\right) V \qquad 7.2.7$$

where $\beta = \sqrt{\frac{2\gamma}{\gamma-1}}$

The positions (O_B) and (1.1) were then obtained from 7.2.2, 6, 7

$$x_{(O_B)} = \left(\frac{4}{\gamma+1}\right)\delta \qquad 7.2.8$$

$$t_{(O_B)} = (O_B)/V \qquad 7.2.9$$

$$x_{(1,1)} = \left(\frac{2\beta}{\beta-1}\right)\delta \qquad 7.2.10$$

$$t_{(1,1)} = \left(\frac{4}{\gamma+1}\right)\left(\frac{\beta+1}{\beta-1}\right)\left(\frac{\delta}{V}\right) \qquad 7.2.11$$

At the head of the Rarefaction Wave:

$$u_Z = V - u_{escape} = \left(\frac{1-\beta}{2}\right) V \qquad 7.2.12$$

$$a_Z = 0 \qquad 7.2.13$$

Let Z = size of the grid, - by trial and error a reasonable pressure drop was obtained by calculating over half the interaction region. The computer was limited to a

grid of 15 by 15 so Z was set at 30 and i and J indexed from 1 to 15.

From 7.2.6, 7, 12, 13

$$u_{(i+1,1)} = u_{(1,1)} - i\left(\frac{u_{(1,1)}-u_Z}{Z}\right) \qquad 7.2.14$$

$$a_{(i+1,1)} = a_{(1,1)}\left(\frac{Z-i}{Z}\right) \qquad 7.2.15$$

Now to obtain $u_{(i,j)}$ and $a_{(i,j)}$ in remaining regions if $i = j$ from 7.2.1, 4, 5, knowing 7.2.14 and 7.2.15

$$u_{(i+1,j+1)} = \left(\frac{1}{1+\beta}\right)\left[u_{(i+1,j)} + \left(\frac{2}{\gamma-1}\right) a_{(i+1,j)}\right] \qquad 7.2.16$$

$$a_{(i+1,j+1)} = \left(\frac{\gamma}{\beta}\right) u_{(i+1)(j+1)} \qquad 7.2.17$$

if $i \neq j$ from 7.2.1 and knowing 7.2.14, 15, 16 and 17

$$u_{(i+2,j+1)} = \frac{1}{2}\left[\left(u_{(i+1,j+1)} + u_{(i+2,j)} + \frac{2}{\gamma-1}\left\{\left(a_{(i+2,j)} - a_{(i+1,j+1)}\right\}\right]\right. \qquad 7.2.18$$

$$a_{(i+2,j+1)} = \frac{1}{2}\left[a_{(i+1,j+1)} + \frac{\gamma-1}{2}\left(u_{(i+2,j)} - u_{(i+1)(j+1)}\right) + a_{(i+2,j)}\right] \qquad 7.2.19$$

The pressures in the regions of interest (i.e. for i + j) from 7.2.3 and knowing 7.2.7 and 19

$$p_{(i+1,j+1)} = p_{(1,1)} \left[\frac{a_{(i+1)(j+1)}}{a_{(1,1)}} \right]^{\frac{2\gamma}{\gamma-1}} \qquad 7.2.20$$

where $p_{(1,1)} = \rho w\, u_s = (\frac{\gamma+1}{8})\, \rho\, v^2$ 7.2.21

To locate the positions $x_{(i,j)}$, $t_{(i,j)}$ knowing $u_{(i,j)}$ and $a_{(i,j)}$ from 7.2.2, 4, 5, and knowing 7.2.8, 9, 10, and 11

$$t_{(i+1,1)} = \frac{1}{2(a_{(i+1,1)}} \left[(x_{(i,1)} - x_{OB}) - u_{(i+1,1)}(t_{(1,1)} - t_{OB}) \right] ..$$

$$.. \quad + \frac{1}{2} \left[t_{OB} + t_{(i,1)} \right] \qquad 7.2.22$$

knowing 7.2.22

$$x_{(i+1,1)} = x_{OB} + (t_{(i+1,1)} - t_{OB})(u_{(i+1,1)} + a_{(i+1,1)}) \qquad 7.2.23$$

if i = j

From 7.2.2, 4 and 5 knowing 7.2.22, 23

$$t_{(i+1,j+1)} = \frac{x_{(i+1,j)} - x_{(i,j)} + (\frac{\gamma+1}{2\gamma})\, \beta a_{(i+1,j+1)} t_{(i,j)}}{\left[\frac{(\gamma+1)\beta - 2\gamma}{2\gamma} \right] a_{(i+1,j+1)} - u_{(i+1,j+1)}} ..$$

$$.. - t_{(i+1,j)}(u_{(i+1,j+1)} + a_{(i+1,j+1)}) \qquad 7.2.24$$

knowing 7.2.24

$$x_{(i+1,j+1)} = x_{(i+1,j)} + \left(u_{(i+1,j+1)} + a_{(i+1,j+1)}\right) \cdots$$

$$\cdots \left(t_{(i+1,j+1)} - t_{(i+1,j)}\right) \qquad 7.2.25$$

if $i \neq j$

From 7.2.2 and knowing 7.2.22, 23, 24 and 25

$$t_{(i+2,j+1)} = \frac{1}{2a_{(i+2,j+1)}} \left[x_{(i+1,j+1)} - x_{(i+2,j)} - u_{(i+2,j+1)} \cdots \right.$$

$$\left. \cdots \left(t_{(i+1,j+1)} - t_{(i+2,j)}\right) + \frac{1}{2} t_{(i+1,j+1)} + t_{(i+2,j)}\right] \qquad 7.2.26$$

knowing 7.2.26

$$x_{(i+2,j+1)} = x_{(i+2,j)} + \left(t_{(i+2,j+1)} - t_{(i+2,j)}\right) \cdots\cdots$$

$$\cdots \left(u_{(i+2,j+1)} + a_{(i+2,j+1)}\right) \qquad 7.2.27$$

From the above analysis u, a, p can be obtained for the regions of interest where i=j. The corresponding position along the shock can be obtained from x and t.

Figure 7.2.3 shows the decay of the shock pressure with pellet length traversed by the shock plotted in the non-dimensional form of $\frac{p}{\frac{1}{2}\rho V^2}$ vs. x/δ. The decay of the pellet shock with pellet length can be seen to be a function of γ, ρ, V, and δ. The shock

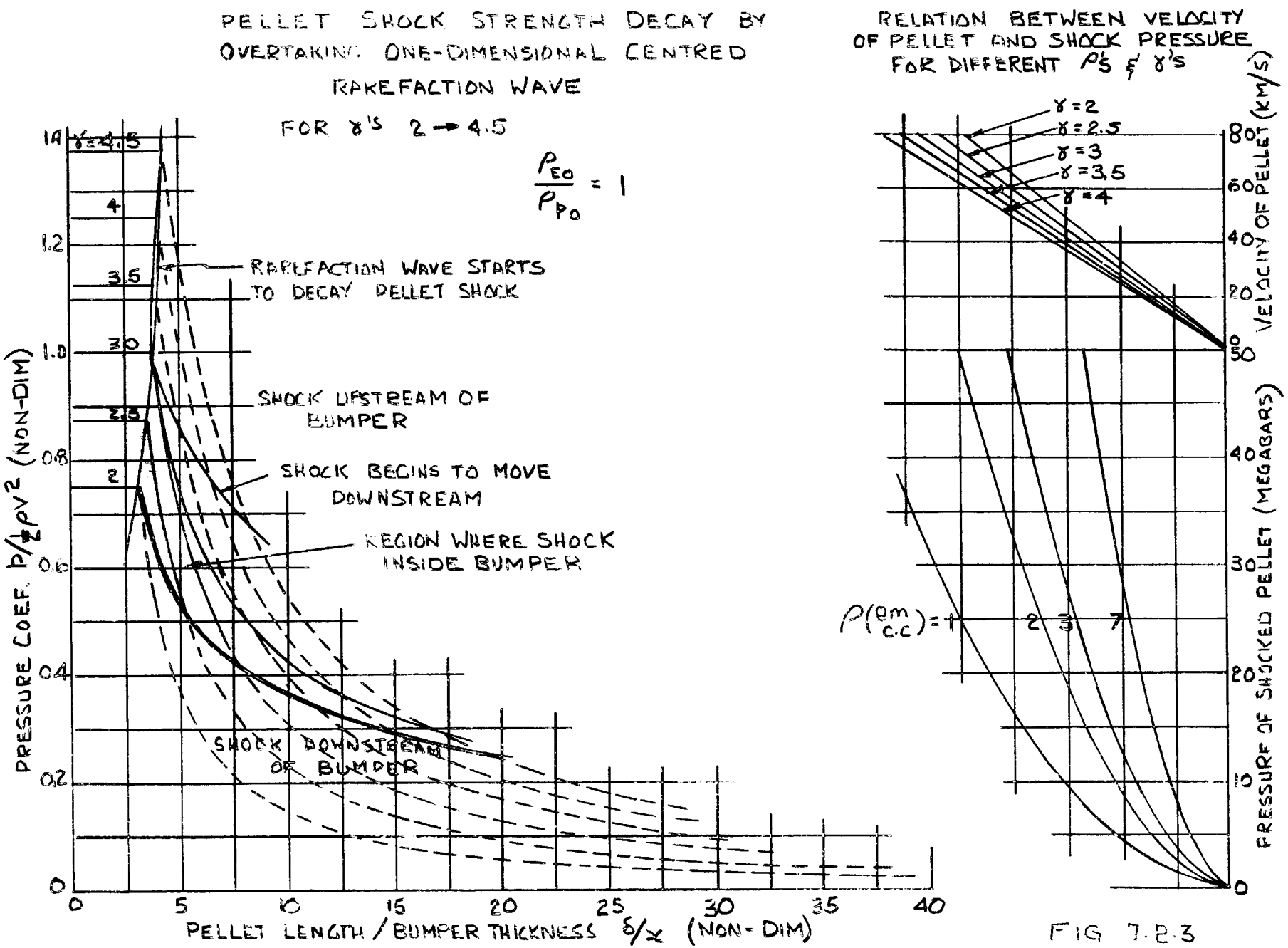
PELLET SHOCK STRENGTH DECAY BY OVERTAKING ONE-DIMENSIONAL CENTRED RAREFACTION WAVE
FOR γ'S 2 → 4.5
$\frac{\rho_{E0}}{\rho_{P0}} = 1$
γ=4.5
4
3.5
3
2.5
2
RAREFACTION WAVE STARTS TO DECAY PELLET SHOCK
SHOCK UPSTREAM OF BUMPER
SHOCK BEGINS TO MOVE DOWNSTREAM
REGION WHERE SHOCK INSIDE BUMPER
SHOCK DOWNSTREAM OF BUMPER
PRESSURE COEF. $P/\frac{1}{2}\rho V^2$ (NON-DIM)
0
0.2
0.4
0.6
0.8
1.0
1.2
1.4
0
5
10
15
20
25
30
35
40
PELLET LENGTH / BUMPER THICKNESS δ/x (NON-DIM)
RELATION BETWEEN VELOCITY OF PELLET AND SHOCK PRESSURE FOR DIFFERENT ρ'S & γ'S
γ=2
γ=2.5
γ=3
γ=3.5
γ=4
$\rho(\frac{gm}{c.c})$ = 1
2
3
7
VELOCITY OF PELLET (KM/S)
0
20
40
60
80
100
PRESSURE OF SHOCKED PELLET (MEGABARS)
0
10
20
30
40
50

FIG 7.2.3

position relative to the bumper is also indicated. For $\gamma > 3$ the shock will initially progress upstream of the bumper then as the shock decays it will pass through the bumper and progress downstream. For $\gamma \leq 2$ the shock will initially pass downstream of the bumper. It should be noted that when the shock is outside the bumper the rate of decay will be greater than shown due to the action of the radial rarefaction waves.

The auxiliary curves on the right of figures 7.2.3 show the relationship between particle velocity and initial pressure for various initial densities and γ's.

It can be seen from figure 7.2.2 that a different analytical solution must be used to determine the positions $x_{(i,1)}$, $t_{(i,1)}$ and the regions $u_{(i,1)}$, $a_{(i,1)}$. Once these values have been determined the same analytical solution used previously for the interaction will be valid if γ_p and ρ_{p_o} are substituted for γ and ρ.

The reflected rarefaction waves from the contact surface were neglected for this analysis in order to remain within the storage requirements of the computer.

The ratio of sound speeds across the contact surface can be obtained from the shocked Mach Numbers (reference 1)

$$\frac{a_p}{a_B} = \left[\frac{\gamma_p(\gamma_p-1)(\gamma_B+1)\,\rho_{BO}}{\gamma_B(\gamma_B-1)(\gamma_p+1)\,\rho_{p_o}} \right]^{1/2}$$

and $$a_p = \left[\frac{\gamma_p - 1}{\gamma_B - 1}\frac{\beta_p}{\beta_B}\right] a_B \qquad 7.2.28$$

where $$\beta_p = \sqrt{\frac{2\gamma_p}{\gamma_p - 1}}$$

$$\beta_B = \sqrt{\frac{2\gamma_B}{\gamma_B - 1}}$$

$$\sigma = \sqrt{\frac{\gamma_B + 1}{\gamma_p + 1}\frac{\rho_{BO}}{\rho_{p_o}}}$$

Position O_B: from 7.2.2

$$x_{OB} = \left(\frac{4}{\gamma_B + 1}\right)\delta \qquad 7.2.29$$

$$t_{OB} = \frac{x_{OB}}{V} \qquad 7.2.30$$

In region $S_{(1)}$

from $u_{s(1)} = V - u_B = u_p$

and $u_p = \sigma u_B$ (ref. 1)

$$u_{s_{(1)}} = \left(\frac{\sigma}{1+\sigma}\right) V \qquad 7.2.31$$

$$a_{s(1)} = \frac{\gamma_B - 1}{2}\beta_B\left(\frac{V}{1+\sigma}\right) \qquad 7.2.32$$

Position $s_{(1)}$

from 7.2.2 and knowing 7.2.29, 30, 31 and 32

$$t_{s(1)} = \frac{\delta - x_{OB}}{a_{s(1)}} + t_{OB}\left(u_{s(1)} + a_{s(1)}\right) \qquad 7.2.33$$

$$x_{s(1)} = \delta + u_{s_{(1)}}\, t_{s(1)} \qquad 7.2.34$$

In region s(i)

Introduce grid size Z and variable i

$$a_{s(i+1)} = a_{s(1)} \left(\frac{Z-i}{Z}\right) \qquad 7.2.35$$

from (1)

$$u_{s(i+1)} = u_{s(i)} - \frac{2}{\gamma_B - 1} \left(a_{s(i)} - a_{s(i+1)}\right) \qquad 7.2.36$$

Position $s_{(i)}$ from 7.2.2

$$t_{s(i+1)} = \frac{x_{s(i)} - x_{OB}}{a_{s(i+1)}} + \frac{u_{s(i+1)}}{a_{s(i+1)}} \left(t_{OB} - t_1\right) + t_{OB} \qquad 7.2.37$$

$$x_{s(i+1)} = x_{OB} + \left(t_{s(i+1)} - t_{OB}\right)\left(u_{s(i+1)} + a_{s(i+1)}\right) \qquad 7.2.38$$

In region (1,1)

from 7.2.28 and maintaining contact surface.

$$u_{(1,1)} = u_{s(1)} \qquad 7.2.39$$

$$a_{(1,1)} = a_{s(1)} \left[\frac{\gamma_p - 1}{\gamma_B - 1} \left(\frac{\beta_p}{\beta_B}\right)\right] \qquad 7.2.40$$

Position (1,1)

from 7.2.2

$$t_{(1,1)} = \frac{x_{s(1)} - \delta - t_{s(1)} \left(u_{(1,1)} + a_{(1,1)}\right)}{\left(\frac{\gamma_p - 1}{2}\right) u_{(1,1)} - a_{(1,1)}} \qquad 7.2.41$$

$$x_{(1,1)} = t_{(1,1)} \left(\frac{\gamma_p + 1}{2}\right) u_{(1,1)} + \delta \qquad 7.2.42$$

In region (i,1)

from 7.2.28 and maintaining contact surface

$$u_{(i+1,1)} = u_{s(i+1)} \qquad 7.2.43$$

$$a_{(i+1,1)} = a_{s(i+1)} \left[\frac{\gamma_p - 1}{\gamma_B - 1} \left(\frac{\beta_p}{\beta_B} \right) \right] \qquad 7.2.44$$

Position (i,1)

from 7.2.2

$$t_{(i+1,1)} = \frac{x_{(i,1)} - x_{s(i+1)} - u_{(i+1,1)} (t_{(i,1)} - t_{s(i+1)})}{2\, a_{(i+1,1)}} + \frac{1}{2} (t_{(i,1)} + t_{s(i+1)}) \qquad 7.2.45$$

$$x_{(i+1,1)} = x_{s(i+1)} + (t_{(i+1,1)} - t_{s(i+1)})(u_{(i+1,1)} + a_{(i+1,1)}) \qquad 7.2.46$$

The equations 7.2.16 to 7.2.27 of the previous analysis will still apply to determine the shock interaction with the now non-centred rarefaction wave in the pellet region.

Figures 7.2.4 to 7.2.6 show the decay of the pellet shock as a function of density ratios from 0.1 - 10 for three values of γ (2.0, 3.0, 4.0). As in figure 7.2.3, the shock pressure decay is plotted in non-dimensional form of $\frac{p}{\frac{1}{2} \rho V^2}$ vs. x/δ. The position of the shock relative to the bumper is also shown. It can

be seen from these curves that the shock pressure decay is less for greater bumper densities and larger bumper thickness.

From the curves 7.2.3 - 7.2.6 the critical length of pellet which will be vapourized by the impact shock can be determined. A very conservative critical pressure of 1.5×10^6 psi was chosen as the value below which the pellet material would not vapourize. The temperature in the plasma was assumed to be above the critical value even with shock decay. Figure 7.2.7 shows the critical pellet length as a function of bumper thickness, impact velocity and density ratio. The minimum weight of bumper can be determined by taking various density ratios and their equivalent bumper thicknesses required to vapourize a given pellet.

It should be remembered that in figures 7.2.3 - 7.2.7 the radial rarefaction waves were not considered and hence the shock decay estimated will be less than would be expected in the actual physical case.

7.2.2 Radial Rarefaction Wave

Without analyzing the effect of the interaction of the radial rarefaction with the pellet shock, the critical pellet length cannot be predicted with confidence. As mentioned in section 7.2.1 for certain

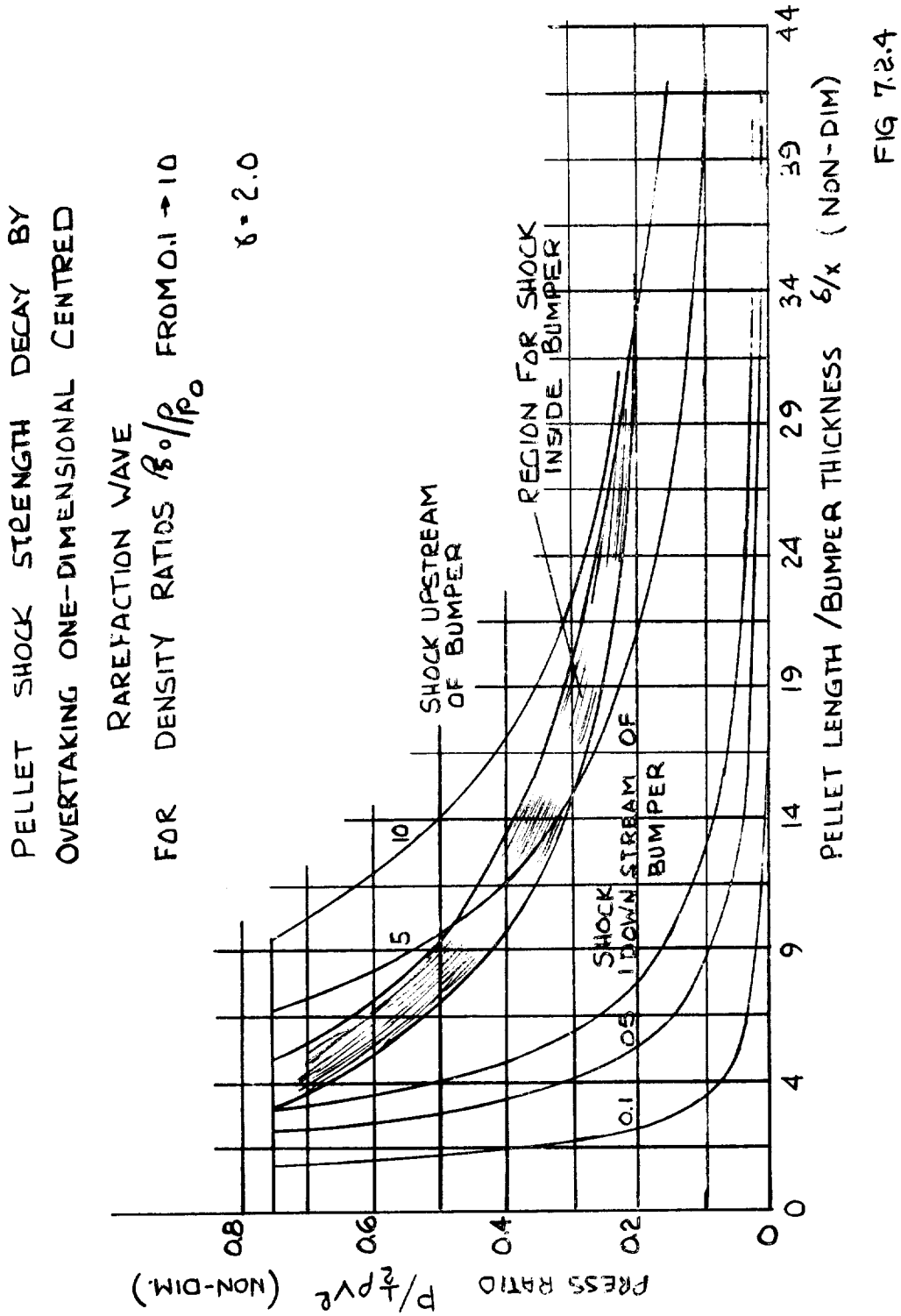
PELLET SHOCK STRENGTH DECAY BY
OVERTAKING ONE-DIMENSIONAL CENTRED
RAREFACTION WAVE
FOR DENSITY RATIOS ρ_0/ρ_0 FROM 0.1 → 10
$\gamma = 2.0$
SHOCK UPSTREAM OF BUMPER
REGION FOR SHOCK INSIDE BUMPER
SHOCK DOWNSTREAM OF BUMPER
10
5
0.5
0.1
PRESS RATIO $P/\frac{1}{2}\rho V^2$ (NON-DIM.)
PELLET LENGTH /BUMPER THICKNESS ℓ/x (NON-DIM)
0
0.2
0.4
0.6
0.8
4
9
14
19
24
29
34
39
44

FIG 7.2.4

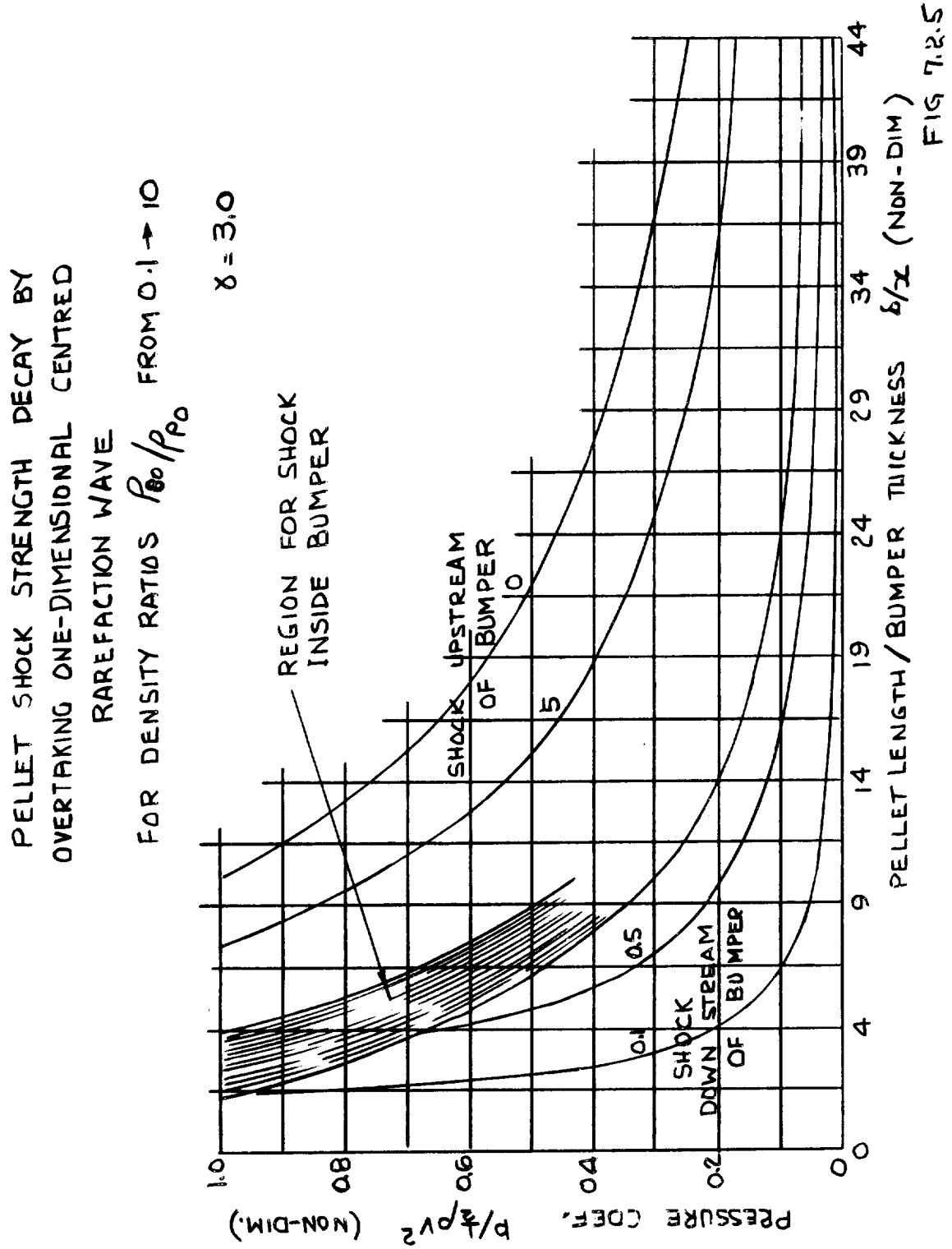
PELLET SHOCK STRENGTH DECAY BY
OVERTAKING ONE-DIMENSIONAL CENTRED
RAREFACTION WAVE
FOR DENSITY RATIOS ρ_∞/ρ_0 FROM 0.1 → 10
$\gamma = 3.0$
REGION FOR SHOCK
INSIDE BUMPER
SHOCK UPSTREAM
OF BUMPER
10
5
0.5
0.1
SHOCK
DOWN
STREAM
OF
BUMPER
PRESSURE COEF. $p/\frac{1}{2}\rho V^2$ (NON-DIM.)
1.0
0.8
0.6
0.4
0.2
0
0
4
9
14
19
24
29
34
39
44
PELLET LENGTH / BUMPER THICKNESS b/x (NON-DIM)

FIG 7.2.5

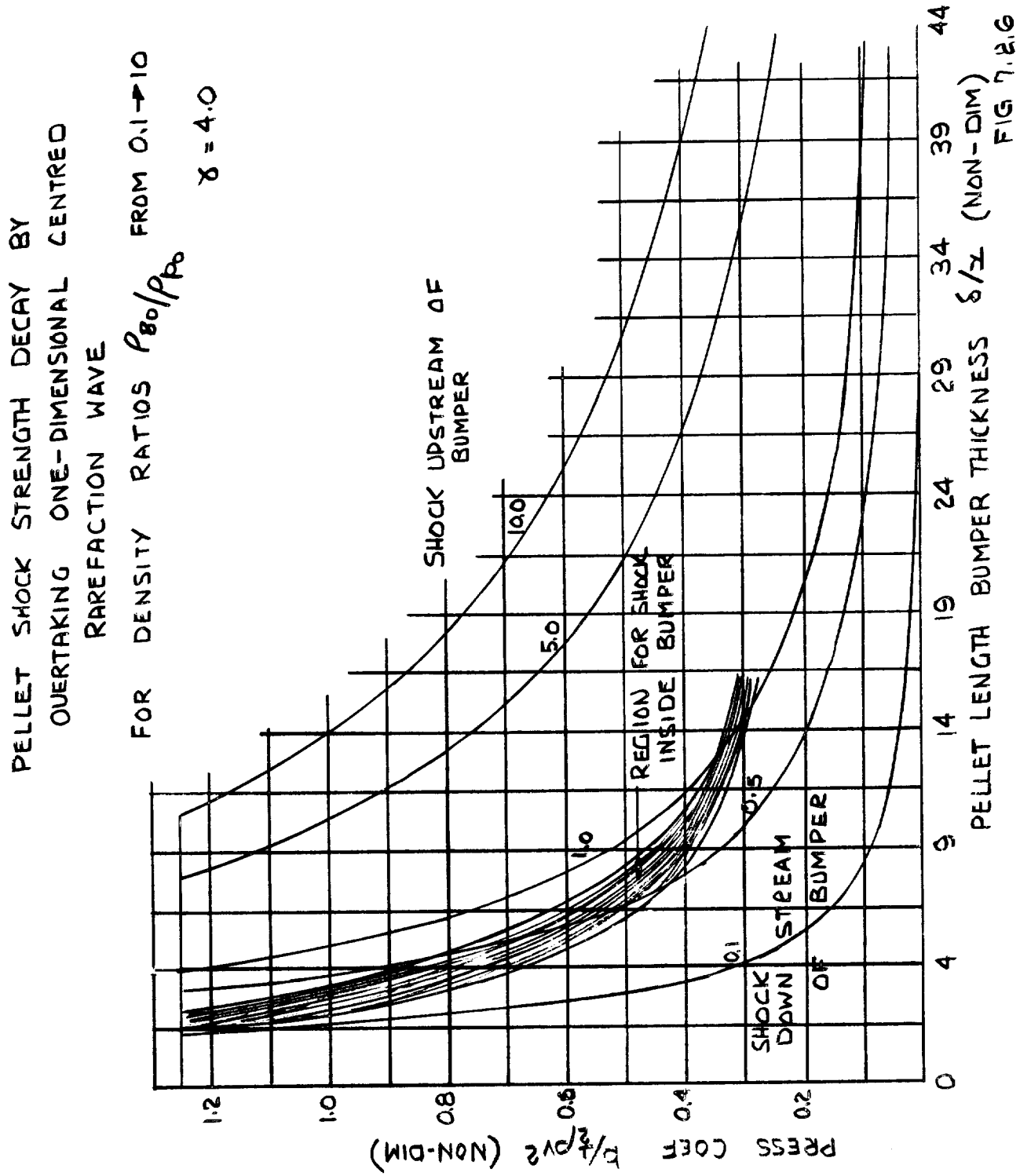
PELLET SHOCK STRENGTH DECAY BY
OVERTAKING ONE-DIMENSIONAL CENTRED
RAREFACTION WAVE
FOR DENSITY RATIOS ρ_{s0}/ρ_{A0} FROM 0.1 → 10
$\gamma = 4.0$
SHOCK UPSTREAM OF BUMPER
100
5.0
1.0
0.5
0.1
REGION FOR SHOCK INSIDE BUMPER
SHOCK DOWN STREAM OF BUMPER
PRESS COEF $p/\frac{1}{2}\rho v^2$ (NON-DIM)
1.2
1.0
0.8
0.6
0.4
0.2
0
4
9
14
19
24
29
34
39
44
PELLET LENGTH BUMPER THICKNESS δ/L (NON-DIM)

FIG 7.2.6

conditions of γ and σ' the shock will initially progress upstream of the bumper for a period of time before being swept downstream through the bumper due to the action of the axial rarefaction wave. During this period of time radial expansion will occur and the radial rarefaction waves will decay the shock.

The mathematical condition for the formation of $\int R$ upstream of the bumper is $(\overleftarrow{V - W_p}) < 0$, where the direction of $\overrightarrow{V}$ is considered positive. The conditions specifying the magnitude and direction of $(\overleftarrow{V - W_p})$ are found by comparing equations 14, 15 and 16 from reference 1, viz.

$$w_p = \frac{\gamma_p + 1}{2} u_p \,, \qquad 7.2.48$$

$$u_B = \frac{V}{1 + \sqrt{\frac{\gamma_B + 1}{\gamma_p + 1} \frac{\rho_{B_o}}{\rho_{p_o}}}} \,, \qquad 7.2.48$$

and

$$\frac{u_p}{u_B} = \frac{1}{\sqrt{\frac{\gamma_p + 1}{\gamma_B + 1} \frac{\rho_{B_o}}{\rho_{p_o}}}} \qquad 7.2.49$$

which when combined yield,

$$w_p = \frac{\gamma_p + 1}{2} \cdot \frac{V}{\sqrt{\frac{\gamma_p + 1}{\gamma_B + 1} \frac{\rho_{p_o}}{\rho_{B_o}} + 1}} \qquad 7.2.50$$

For convenience, set

$$\sigma'^2 = \frac{\gamma_p + 1}{\gamma_B + 1} \frac{\rho_{p_o}}{\rho_{B_o}} , \qquad 7.2.51$$

Noting that if $\frac{\gamma_p + 1}{\gamma_B + 1} \approx 1$, then $\sigma' \approx \sqrt{\frac{\rho_{p_o}}{\rho_{B_o}}}$; note also that for most combinations of pellet/bumper combinations considered, and for low density meteoric impacting on metallic bumper plates,

$$\sigma' \leq 1.$$

Thus,

$$w_p = \frac{\gamma_p + 1}{\sigma' + 1} \frac{V}{2} , \qquad 7.2.52$$

$$u_p = \frac{V}{\sigma' + 1} \qquad 7.2.53$$

$$a_p = \sqrt{\frac{\gamma_p(\gamma_p - 1)}{2}} \frac{V}{\sigma' + 1} , \qquad 7.2.54$$

and

$$(V - w_p) = \left(1 - \frac{1}{2} \frac{\gamma_p + 1}{\sigma' + 1}\right) V. \qquad 7.2.55$$

For $w_p > V$, $\frac{\gamma_p + 1}{\sigma' + 1} > 2$

or

$$\gamma_p > 2\sigma' + 1 \qquad 7.2.56$$

If the pellet and bumper have equal densities and γ's, then for $(V - w_p) < 0$, $\gamma > 3$. If the bumper material is more dense than the pellet and $(\gamma_p + 1)/(\gamma_B + 1) \approx 1$, then $\sigma' < 1$ and $(V - w_p) < 0$ for $\gamma < 3$. For very light meteors impacting on, say, an aluminized mylar bumper, σ' may be

very small so that $(V-w_p) < 0$ for any real value of γ' ; viz. for $\sigma' = 0.1$, $w_p > V$ for $\gamma_p' \geq 1.2$. From the point of view of eliminating the cylindrical rarefaction decay it is apparent that $\sigma' \geq 1$ is desired, however, since the strength of $\overleftarrow{S_p}$ and hence its destructive power is inversely proportional to σ', the length of pellet destroyed for any given V is also inversely proportional to σ'.

Consider the following sketch, (figure 7.2.7). The disturbance originating at position (o, y_o) at time t=o will, after a time dt, be characterized by a circular front of radius a_p dt, centred at $((V-u_p)dt, y_o)$. The

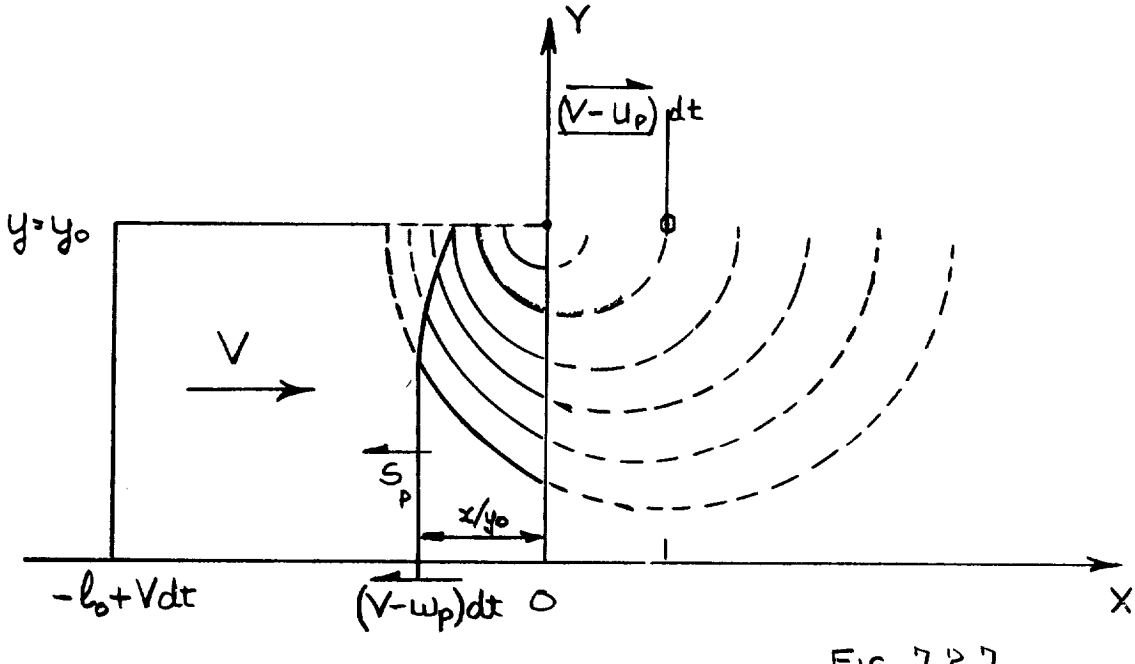

FIG 7.2.7

circular front then is described by

$$(x - (\overrightarrow{V-u_p})\ dt)^2 + (y-y_o)^2 = a_p{}^2\ dt^2 \qquad 7.2.57$$

at time dt.

The position of the shock $\overleftarrow{S_p}$ at time dt is given by

$$x = \overleftarrow{(V - w_p)}\ dt \qquad 7.2.58$$

The point of interaction of the shock and the head of the rarefaction, is found by combining 7.2.57 and .58 to yield

$$y = y_o + \sqrt{a_p{}^2 - (w_p-u_p)^2}\ dt\ ;\ x = (V-w_p)dt \qquad 7.2.59$$

The point at which the influence of $\sqrt{R_C}$ has been extended to include the entire shock wave, that is, where the head of $\sqrt{R_C}$ intercepts $\overleftarrow{S_p}$ at y=o, is given by

$$y_o = -\sqrt{a_p{}^2 - (w_p - u_p)^2}\ dt \qquad 7.2.60$$

$$x = \frac{-(V-w_p)\ y_o}{\sqrt{a_p{}^2 - (w_p-u_p)^2}} \qquad 7.2.61$$

This reduces to

$$\frac{x}{y_o} = \frac{\gamma+1 - 2(\sigma+1)}{\sqrt{(\gamma+1)(\gamma-1)}} \qquad 7.2.62$$

when 7.2.61 is combined with equations 14 - 16 of reference 1 and equation no. 7.2.51.

Figure 7.2.8 is a plot of x/y_o vs. γ and σ' (solid lines). Note that (x/y_o) is measured from the bumper plate front face and thus gives the distance between that face and $\overleftarrow{S_p}$ for complete influence by $\sqrt{R_c}$.

The position of the wave $\overleftarrow{S_p}$ from the rear face of the pellet for the above situation, assuming the pellet length is ℓ_o, is given by

$$\frac{x}{y_o} = \ell_o - \sqrt{\frac{\gamma+1}{\gamma-1}}\, y_o \qquad 7.2.63$$

since in the time dt taken by the wave to reach the pellet centre line the pellet has moved a distance

$$Vdt = \frac{V\, y_o}{\sqrt{a_p^2 - (w_p-u_p)^2}} = \frac{2\,(\sigma+1)}{\sqrt{(\gamma-1)(\gamma+1)}} \qquad 7.2.64$$

Note that σ' does not appear in this expression, hence the overtaking and decay of $\overleftarrow{S_p}$ by $\sqrt{R_c}$ is independent of the pellet and bumper densities, and depends only on γ_p. In figure 7.2.8 equation 7.2.63 is shown (dotted lines) along with equation 7.2.62. Note that for $\gamma = 3$, regardless of the density ratio, over 70% of the pellet is consumed by $\overleftarrow{S_p}$ (at the pellet axis) before feeling the influence of $\sqrt{R_c}$, if $\ell_o = 2y_o$.

For $\gamma = 3$, $\sigma' = 1$, $(x/y_o)_{rel} = 0$, that is, $\overleftarrow{S_p}$ remains fixed at the exit plane. For $\gamma = 3+\varepsilon$ where

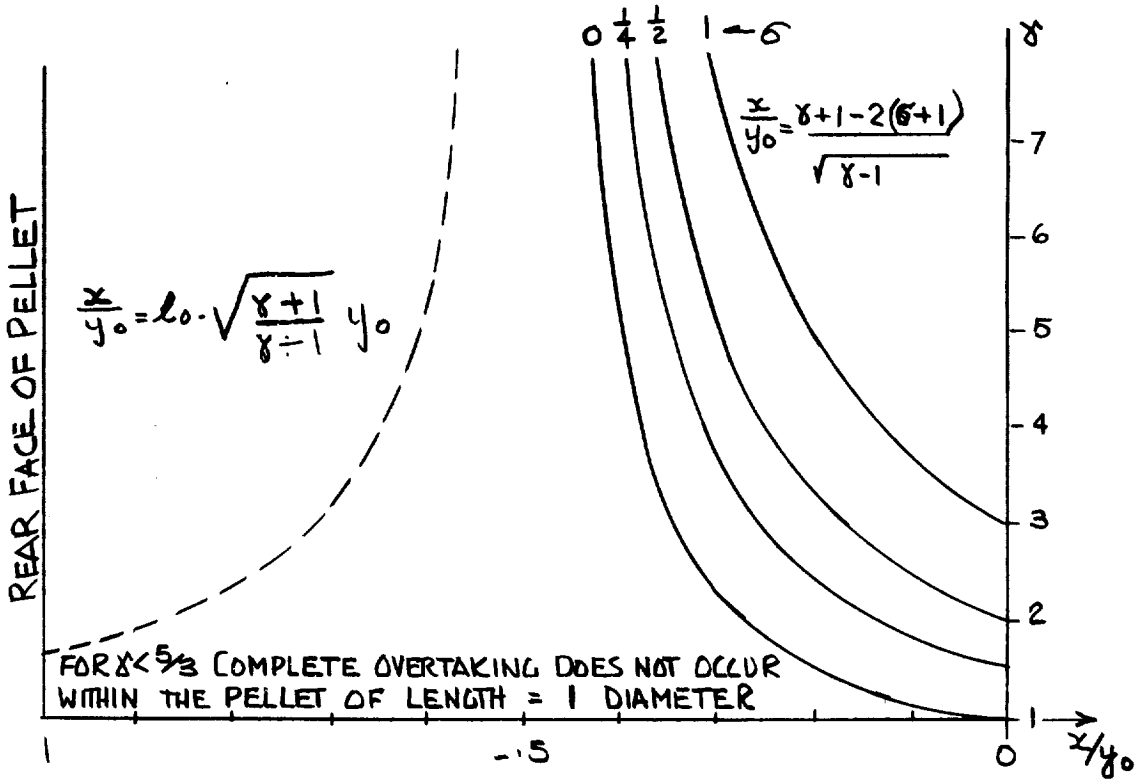

Distance to dotted line (measured from $x/y_o = 0$) represents the absolute distance travelled by the shock $\overleftarrow{S_p}$ before the rarefaction wave $\sqrt{R_c}$ indluences the entire shock. Note that this distance is a function of γ only not of σ (equation 7.2.63).

Distance do solid line represents the distance relative to the front face of the bumper plate travelled by $\overleftarrow{S_p}$ before being influenced entirely by $\sqrt{R_c}$ (as function of both γ and σ)(equation 7.2.62).

INTERACTION BETWEEN $\overleftarrow{S_p}$ & $\sqrt{R_c}$ UPSTREAM OF BUMPER

FIG 7.2.8

$\varepsilon << 1$ $\overleftarrow{S_p}$ also remains essentially fixed at the impact plane $x = -\delta$, however, an $\sqrt{R_c}$ wave is generated since, in fact, the position of $\overleftarrow{S_p}$ is $x = -(\delta + \varepsilon t)$. Some radial pellet flow must occur on the front face of the bumper for $\gamma = 3 + \varepsilon$, thus the pellet shock must experience decay by the action of the cylindrical expansion.

The above analysis is valid only if the cylindrical expansion is assumed to emanate from the point $x = -\delta$, $y=y_o$ on figure 7.2.1, that is, at the geometrical junction between the front face of the bumper and the pellet periphery. If, as is most probable in any real interaction, the pellet is destroyed at the periphery by $\overleftarrow{S_p}$ as well as in its interior, the origin of $\sqrt{R_c}$ will follow some distance behind $\overleftarrow{S_p}$, the lag depending on the ratio of the rates of radial to axial decay. The head of $\sqrt{R_c}$ will not be affected by the motion of the point of origin, but its internal structure and hence the rate of radial and axial decay of $\overleftarrow{S_p}$ will be influenced by this factor.

As the edge of the pellet shock decays, due to radial rarefaction wave interaction, it's speed will fall and it will tend to move back into the bumper, so cutting off the rarefaction. In fact, the pressure behind the shock will fall until the velocity equals that of the pellet and the shock will remain a short

distance ahead of the bumper, leaving a narrow slot for the high pressure gas to escape. The pressure behind the outer edge of the shock required to maintain this shock speed will be $(\frac{2}{\gamma+1})\rho_o V^2$ from equation 5 of reference 1, setting $w_p = V$; for $\gamma = 4$, the initial shock pressure $(\frac{\gamma+1}{8}\rho_p V^2)$ is $\frac{5}{8}\rho_p V^2$, and the ratio of pressure behind the decayed shock to that behind the undecayed shock is 16/25 or .64. As the main part of the shock gets further ahead of the edge and the shock surface becomes inclined to the pellet velocity, the shock can decay further, as seen in figure 7.2.9. If the shock stabilized at some angle θ, so then $w_p = V\cos\theta$. $P = \frac{2}{+1}\rho_{po} V^2 \cos^2\theta$. and if $\theta = 45^\circ$, the shock pressure will have dropped by a further factor of two.

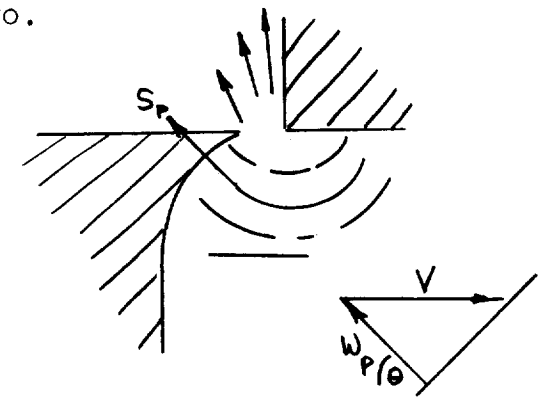

FIG. 7.2.9

From the analysis of the interaction of the reflected rarefaction with the shock, the shock travels a distance of about 1.5 bumper thicknesses before reversing direction, so that for thin bumpers, the

angle θ is likely to be less than 45°. Consequently the shock decay by a cylindrical rarefaction ahead of the bumper is not likely to be the limiting factor in pellet destruction.

The shock will eventually pass downstream of the bumper in all cases due to the interaction with the axial rarefaction wave. The length of pellet that will be shocked before the radial rarefaction wave downstream of the bumper reaches the centre of the pellet can be determined from the previous axial and radial rarefaction wave analysis. The time for the pellet shock to move just downstream of the bumper and the shocked state at this moment can be obtained from figures 7.1.3 - 7.1.7 for the axial rarefaction interaction with the shock. Then using the analysis for the radial rarefaction interaction equations 7.2.13 - 7.2.17 the length of pellet fed into the pellet shock before the radial rarefaction reaches the centre of the pellet can be calculated. Figure 7.2.10 shows the length of pellet that is shocked as a function of the radius of the pellet and γ for $\sigma = 1$.

It can be seen from figure 7.2.10 that the radial rarefaction wave downstream of the bumper will not reach the centre of the pellet before it is consumed if it has an L/D ratio less than 2. (taking $\sigma = 1$ and $\gamma \geq 2$). It is certain that, as long as the pressure in the core

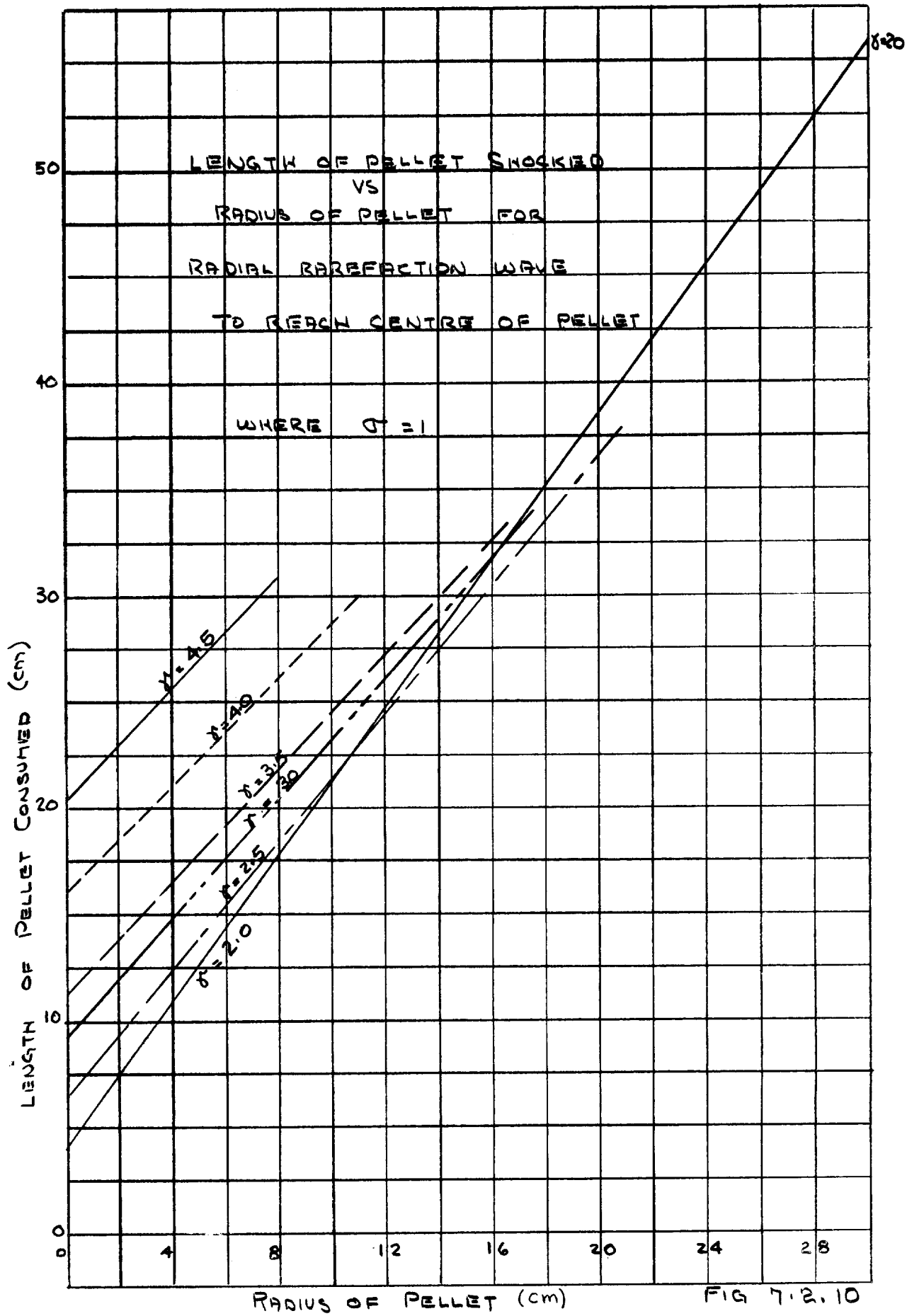
LENGTH OF PELLET SHOCKED
VS
RADIUS OF PELLET FOR
RADIAL RAREFACTION WAVE
TO REACH CENTRE OF PELLET
WHERE σT = 1
γ = 4.5
γ = 4.0
γ = 3.5
γ = 3.0
γ = 2.5
γ = 2.0
γ = 1.0
LENGTH OF PELLET CONSUMED (cm)
RADIUS OF PELLET (cm)
0
10
20
30
40
50
4
8
12
16
20
24
28

FIG 7.2.10

of the shocked pellet and inside the radial rarefaction wave is of the order of a million pounds per square inch any unvapourized skin which might result from edge decay of the shock will be fragmented as a result of this internal pressure. Therefore it has been assumed for the present that the decay of the pellet shock due to the radial rarefaction waves will not limit the critical length of pellet providing the L/D ratio of the pellet is < 2. A computer program is now being written for the decay of the pellet shock due to the radial rarefaction wave interaction based on a stepwise analysis in the radial and axial directions.

7.3 Long Term Expansion

The analytical and numerical analyses for the expansion of the gas flow in the one and two dimensional regions behind the bumper are limited by the assumption that pellet material is continually feeding into the pellet shock and thereby supplying compressed material to the expansion wave. For short pellets (L/D = 1-2) the gas cloud is still less than two diameters behind the bumper when the last of the pellet is vapourized by the shock; after this the gas cloud expands without a continuous supply of shock material.

The gas flow expansion for large distances downstream of the bumper was analysed approximately using the method of Stanyukovich (Ref. 5) for the expansion of a sphere of compressed gas into a vacuum. This approximation may be seriously in error if the plasma produced by the impact exhibits considerable cohesion and acts more like a fluid metal being bound together by the free electrons in the lattice of positive ions, than a gas (ref. 7). However Bauer, Cook and Keyes (Ref. 8) show that if a detonation generated plasma is compressed, on subsequent expansion it overexpands past its equilibrium size, becomes unstable as recombination occurs, and explodes. If this explosion occurs in all directions, then the expanding sphere analysis would seem to be a useful one.

The instant the spherical boundary of a compressed gas is released into a vacuum a rarefaction wave is initiated at the original boundary. The particles originally forming the boundary travel outwards at escape velocity while the head of the wave will move into the compressed gas at the local speed of sound, until it reaches the centre. Up to this time the material enclosed by the wave head is unchanged. Once the wave reaches the centre it will be reflected as a

spherically expanding rarefaction (without such a reflected wave an expanding void would be produced at the centre), and the density inside the wave then decreases with time.

Stanyukovich discusses the distribution of density and velocity in the gas cloud both for short times before the head of the rarefaction wave reaches the centre, and for long times when general decay has taken place. An analytical solution is apparently impossible (p. 498, Ref. 5) but several approximations are suggested, appropriate to various times. Since a long time solution was required for this analysis equations 63.22 and 63.23 were used, taking N=2 for spherical symmetry.

$$u_r = r/t \quad \text{for } r \leq a_o t \quad \text{i.e. } r_{max} \qquad 7.3.1$$

$$u_r = o \quad \text{for } r > a_o t$$

and

$$\rho = \frac{A\, M_o}{(a_o t)^3} \left[1 - \left(\frac{\gamma - 1}{2} \frac{r}{a_o t}\right)^2\right] \qquad 7.3.2$$

where A and Y were evaluated by Stanyukovich using the conservation of mass and energy.

$$Y = 3\gamma + Z \qquad 7.3.3$$

$$A = \frac{(2Y+3)!}{Y!\,(Y+1)!\,2^{(2Y+1)}} \left(\frac{\gamma - 1}{2}\right)^3 \frac{1}{4\pi} \qquad 7.3.4$$

M_o, the total mass remains constant.

Momentum is not conserved in the above equation for density but Stanyukovich estimates a maximum error of only +10%. The accuracy of his equations could be checked by programming an expanding sphere based on the conservation of mass, momentum and energy.

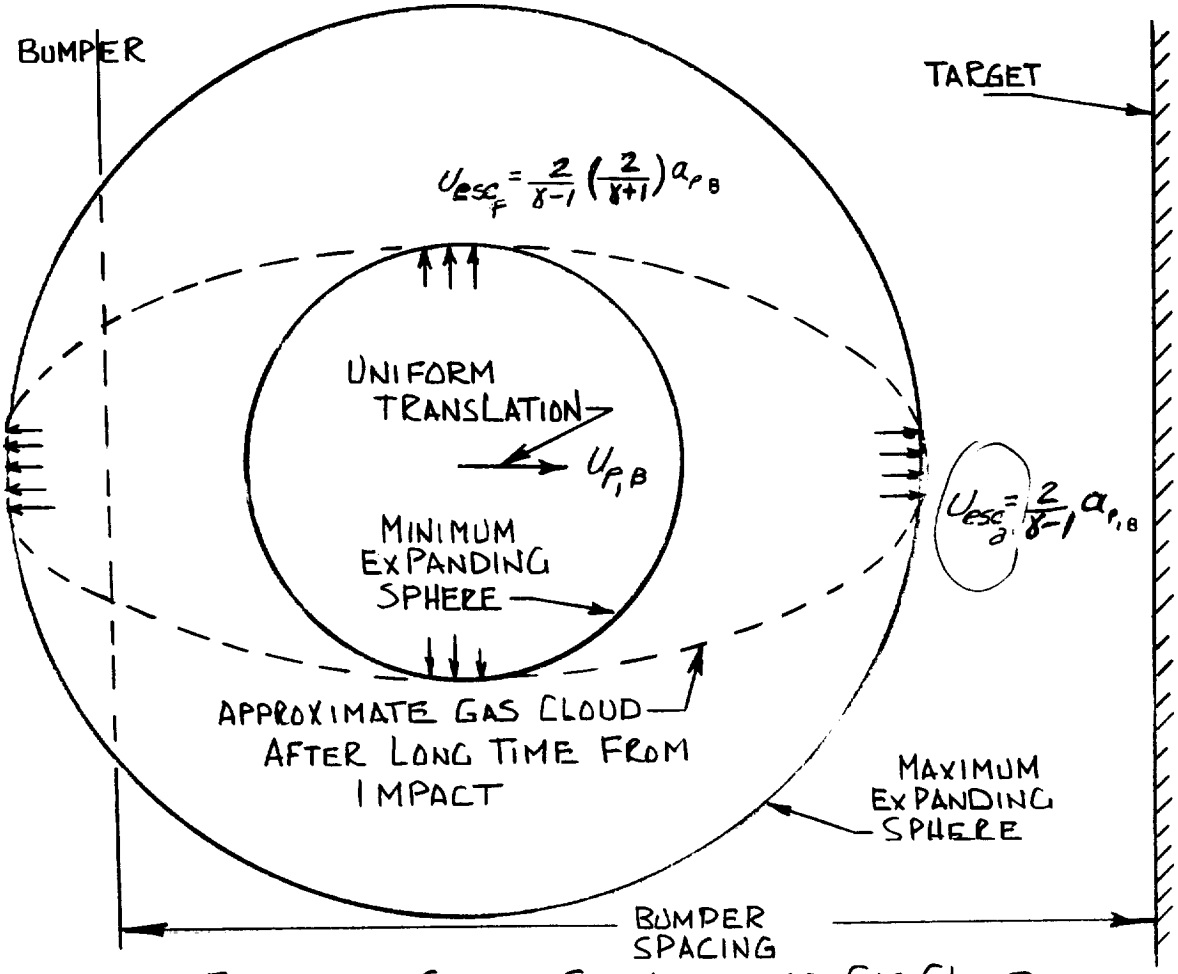

EXPANDING SPHERE SIMULATION OF GAS CLOUD

FIG 7.3.1

It is not possible to use a single expanding sphere approximation, because it does not match the short-time flow given by the cavity-flow model. This model showed that the axial escape velocity to the right was $\left(\frac{2}{\gamma-1}\right) a_{P,B}$ (which will also be that to the left), whereas

the radial escape velocity is $\frac{2}{\gamma-1}\left(\frac{2}{\gamma+1}\, a_{P,B}\right)$. The gas cloud will therefore have the approximate shape of an ellipsoid with an eccentricity of 2, if $\gamma = 3$. To estimate the momentum distribution with time and radius at various large distances behind the bumper, the flow in two spheres was calculated, one expanding $\frac{2}{\gamma+1}$ times as fast as the other, as shown in figure 7.3.1. Along the axis, the initial rise in momentum density and flux is given by the larger sphere. However, this model underestimates the density for later times, since it assumes a much greater expansion of the cloud, and the momentum flux and density are obtained from that of the "inscribed" sphere distribution, allowing for the fact that this model overestimates the density.

Only the axial component of momentum was calculated, the radial component may give rise to some scouring but the pressure generated on the witness plate will be the result of the axial component only.

Referring to figure 7.3.2 the centre of the sphere was assumed to be moving to the right with a velocity of u_o; the velocity of the shocked material. This assumption is valid only if the shock strength decay is neglected. A computer program was set up to determine the stagnation pressures a witness plate would experience from the following numerical analysis.

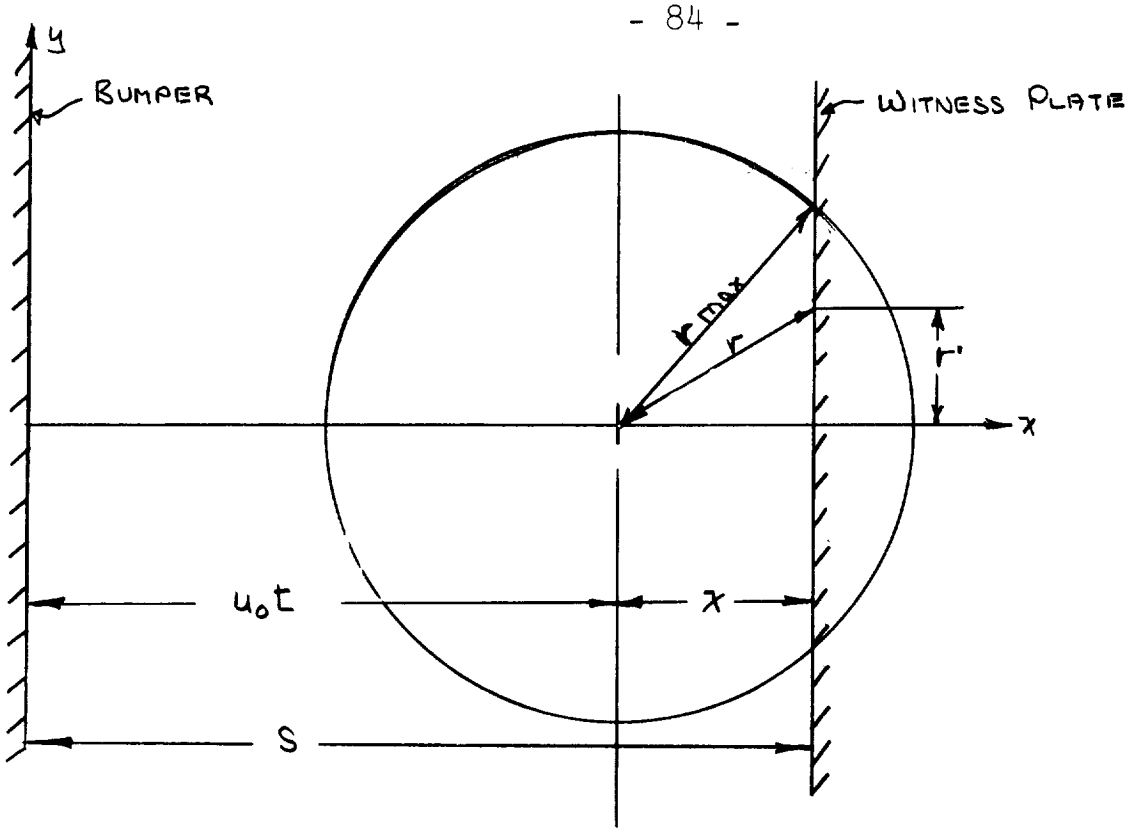

FIG 7.3.2

Values of γ, ρ_{B_o}, V, D, and S were chosen for typical ranges that would be expected in meteor impact, i.e. $\gamma = 2 \rightarrow 3.33$, $\rho_{B_o} = 3$ gm/cm^3, V = 20 - 80 km/sec, D = 1 cm, S = 10 $\rightarrow$ 300 cm. From these given values the constants, u_o, a_o, ρ_o, Y, A, t_i, Δt, and M_o can be calculated as follows.

$$u_o = \frac{V}{2} \quad \text{assuming } \rho_{P_o} = \rho_{B_o} \qquad 7.3.5$$

$$a_o = u_o \sqrt{\frac{\gamma(\gamma-1)}{2}} \qquad 7.3.6$$

$$\rho_o = \rho_{B_o} \left(\frac{\gamma+1}{\gamma-1}\right) \quad \text{assuming limiting density ratios} \qquad 7.3.7$$

$$Y = 3\gamma + 2 \quad \text{Stanyukovich} \qquad 7.3.8$$

$$A = \frac{(2Y + 3)!}{Y!(Y+1)!2^{(2\gamma+1)}} \left(\frac{\gamma-1}{2}\right)^3 \frac{1}{4\pi}$$

Stanyukovich 7.3.9

$$t_i = \frac{s}{u_o + \frac{2}{\gamma-1} a_o} \qquad 7.3.10$$

$$\Delta t = \frac{1}{10} \left(\frac{a_o}{u_o}\right) t_i \left(\frac{2}{\gamma-1}\right)$$

for centre of sphere to reach plate in 10 Δt 7.3.11

$$M_o = \left(\frac{4}{3}\pi \frac{D^3}{8}\right) \rho_o$$

assuming shocked plasma originally occupies a spherical volume with a radius D/2 7.3.12

Now, knowing the above constants, the stagnation pressure for a sphere on the witness plate can be determined as a function of time and radius from the centre axis of the sphere travelling in the directions of impact.

at any time $t = t_i + n\,\Delta t$

where n varies from 1 - 20

$x = s - u_o t$

$r_{max} = a_o t \left(\frac{2}{\gamma-1}\right)$

$r'_{max} = \sqrt{r^2_{max} - x^2}$

$\Delta r' = r'_{max}/10$

where r'_{max} is divided into 10 increments

and at any $r' = m \Delta r'$

where m varies from 1 - 10

$$\rho = \frac{M_o A}{(Y_{max})^3} \left(1 - \frac{r^2}{r^2_{max}}\right)^Y \left(\frac{2}{\gamma - 1}\right)^3$$

for $r_{max} = \frac{2}{\gamma - 1} a_o t$ 7.3.13

$$u = \frac{x}{T} + u_o$$

axial momentum density $= \rho u$ 7.3.14

axial momentum flux $= \rho u^2$ 7.3.15

and stagnation pressure $p_o = \frac{1}{2}\rho u^2 + p$ 7.3.16

where $p = \frac{\rho}{\gamma} a^2$ 7.3.17

and $a = a_o \left(\frac{\rho}{\rho_o}\right)^{\frac{\gamma - 1}{2}}$ 7.3.18

A new value for $a_o = a_o \left(\frac{2}{\gamma + 1}\right)$ is then calculated for the expansion of the small sphere and the computations repeated.

The peak stagnation pressure for the small (radial expansion) sphere and the large (longitudinal expansion) sphere were then plotted as a function of the time after impact for 6 values of γ (1.67 - 3.33), (figures 7.3.3 - 7.3.8). The stagnation pressure for the elliptical expansion was then sketched in by hand with the large sphere expansion dominating at the

extreme ends of the expansion and the small sphere dominating at the centre. It can be seen from figures 7.3.3 - 7.3.8 that the smaller the value of δ' the more accurate will be the approximation to the elliptical expansion.

Figure 7.3.9 shows the non-dimensional peak centreline pressure coefficient $\frac{p_o}{\frac{1}{2}\rho_{B_o} V^2} (\frac{s}{D})^3$ variation with the non-dimensional time coefficient $t/(s/D)$ for various values of δ'. The maximum pressure and the maximum rate of application of pressure on the witness plate can be determined from this figure for known values of ρ_{B_o}, S, D, and V. It can be seen that the peak pressure and rate of application will increase as δ', ρ, V, D increase and s decreases.

Figure 7.3.10 shows the radial distribution of the peak pressure of the expanding ellipse for a particular case with different values of δ'. The radial distribution indicates a general Gaussian error curve which varies approximately as the cube of the radius. The integration of the area under the curve would give the maximum total force acting on the witness plate.

Figure 7.3.11 shows the variation in peak pressure vs. spacing for two impact velocities. The

CENTRE LINE PRESSURE VS TIME AFTER IMPACT

FOR $\gamma = 1.67$

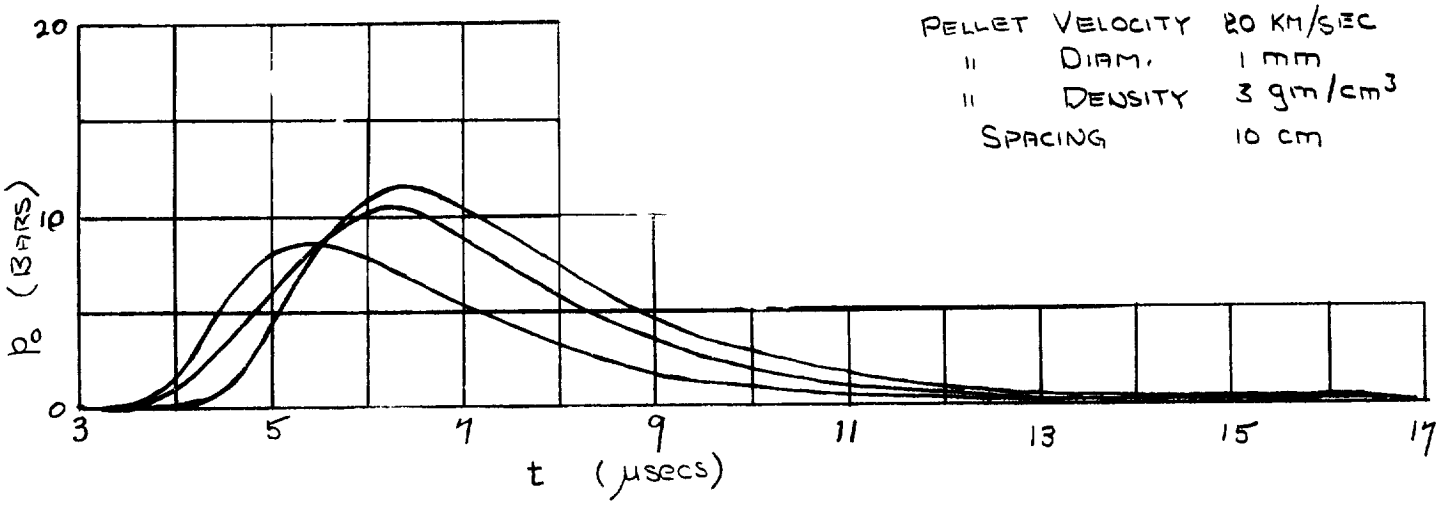

FIG. 7.3.3

CENTRE LINE PRESSURE VS TIME AFTER IMPACT

FOR $\gamma = 2.0$

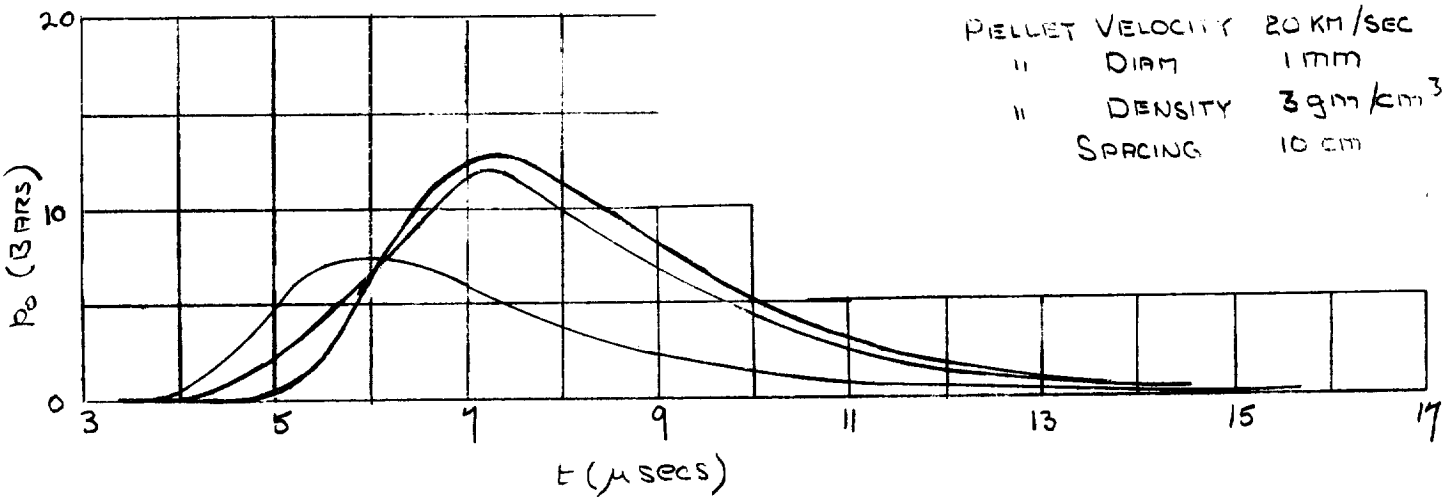

FIG. 7.3.4

CENTRE LINE PRESSURE VS TIME AFTER IMPACT

FOR $\gamma = 2.33$

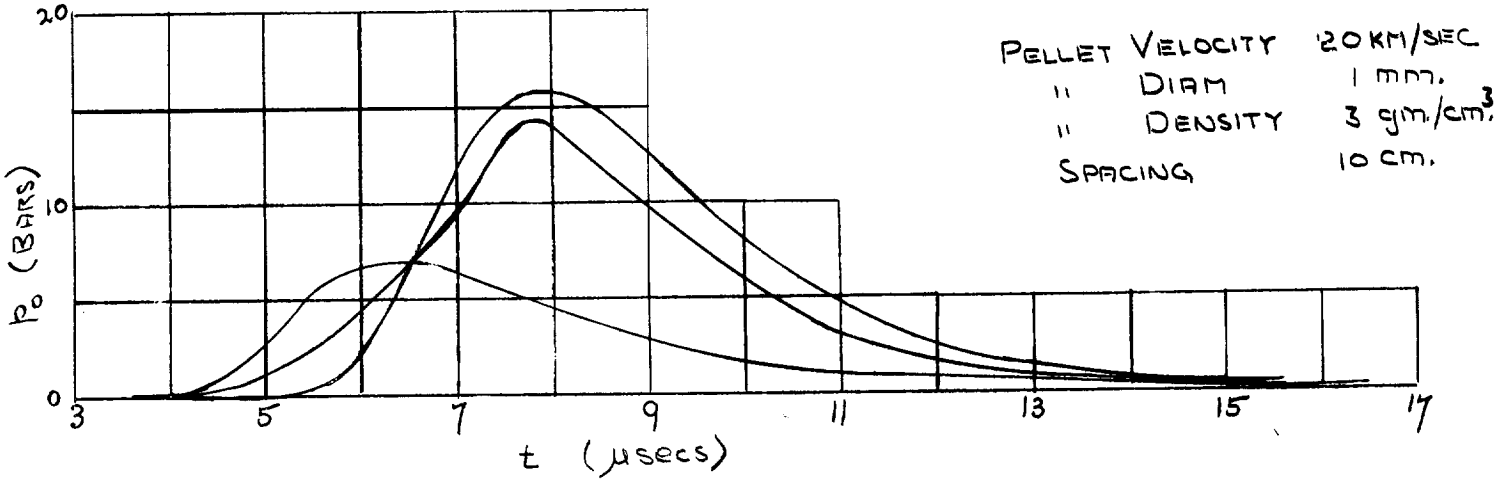

FIG. 7.3.5

CENTRE LINE PRESSURE VS TIME AFTER IMPACT

FOR $\gamma = 2.67$

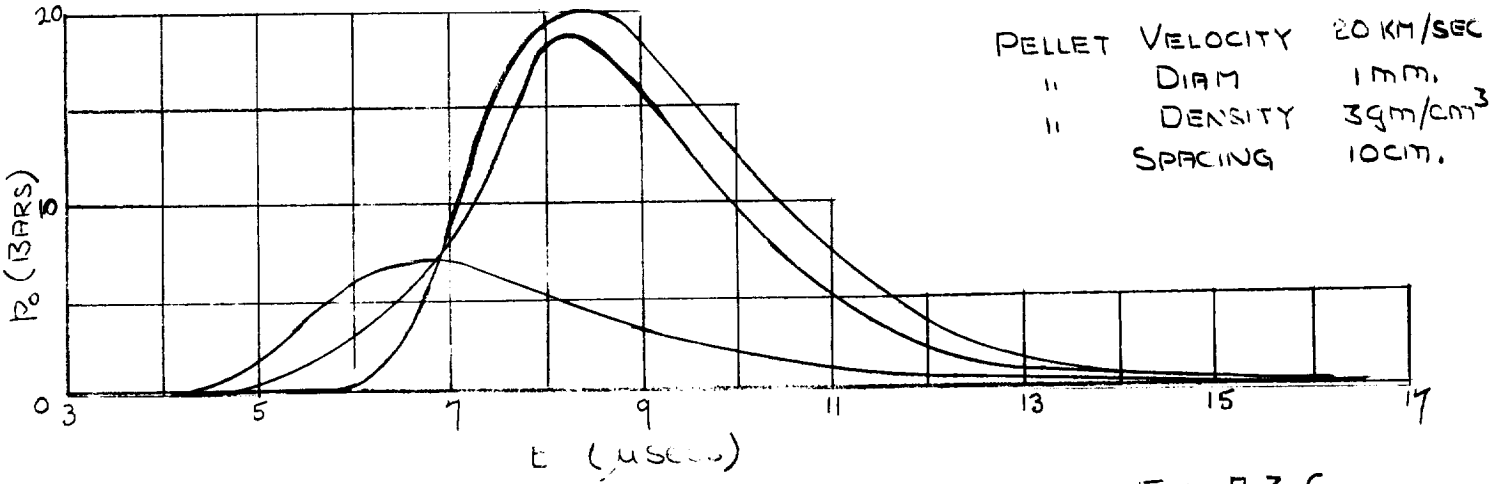

FIG. 7.3.6

CENTRE LINE PRESSURE VS TIME AFTER IMPACT

FOR $\delta' = 3.0$

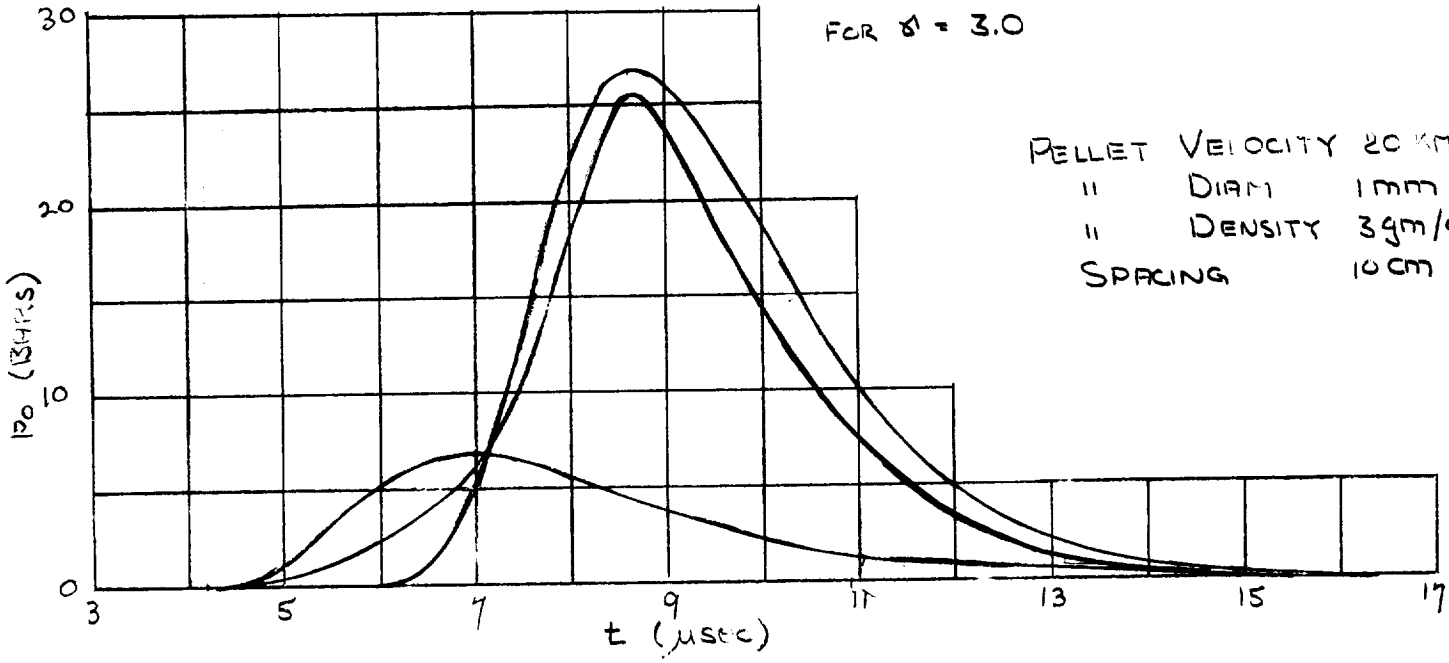

PELLET VELOCITY 20 KM/sec
" DIAM 1 mm
" DENSITY 3 gm/cm^3
SPACING 10 cm

FIG 7.3.7

CENTRE LINE PRESSURE VS TIME AFTER IMPACT

FOR $\delta' = 3.33$

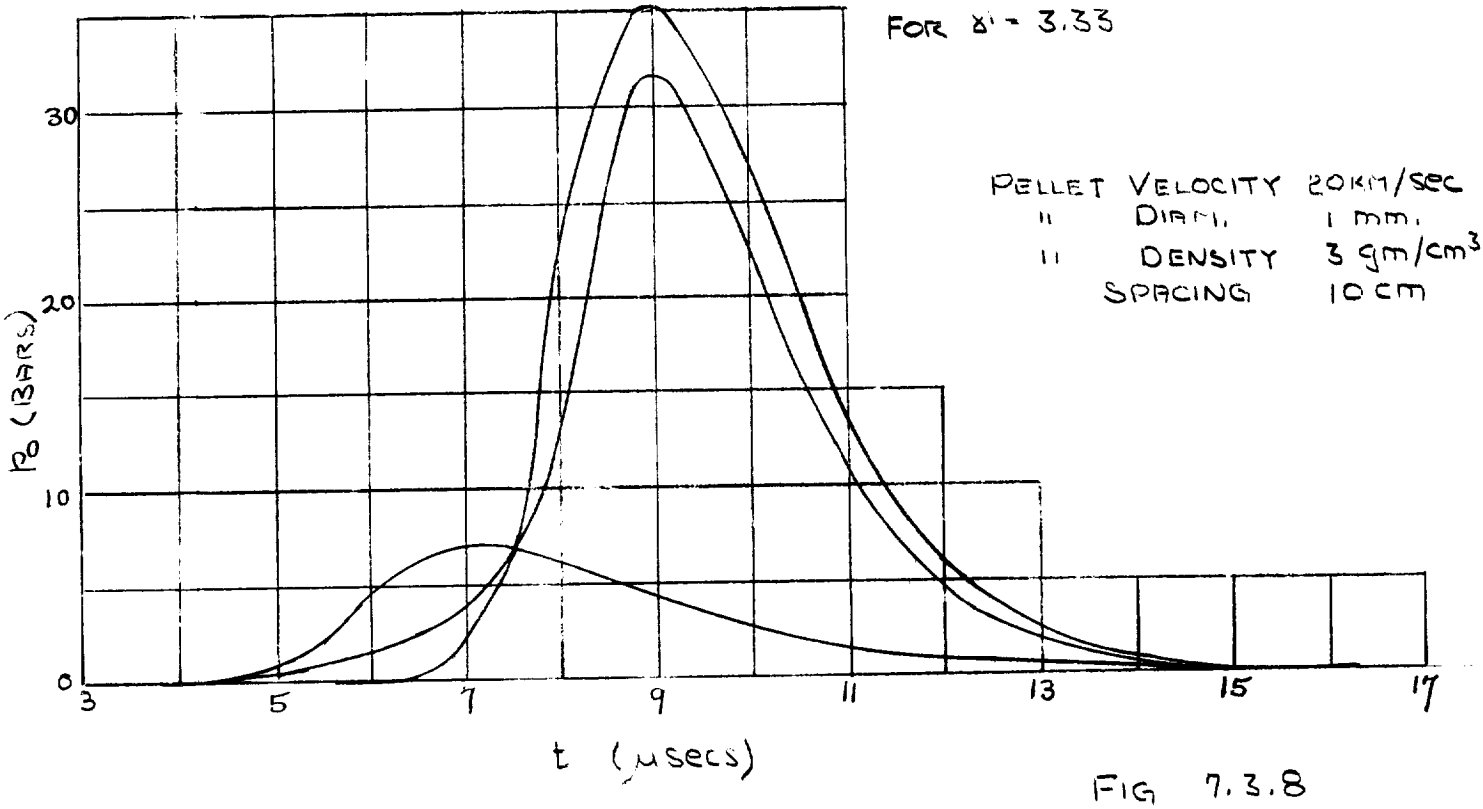

PELLET VELOCITY 20KM/sec
" DIAM. 1 mm.
" DENSITY 3 gm/cm^3
SPACING 10 cm

FIG 7.3.8

EXPANDING SPHERE ANALYSIS FOR S > 2D

CENTRE LINE PRESSURE COEFF. VS TIME COEFF.

FOR γ 1.67 → 3.33

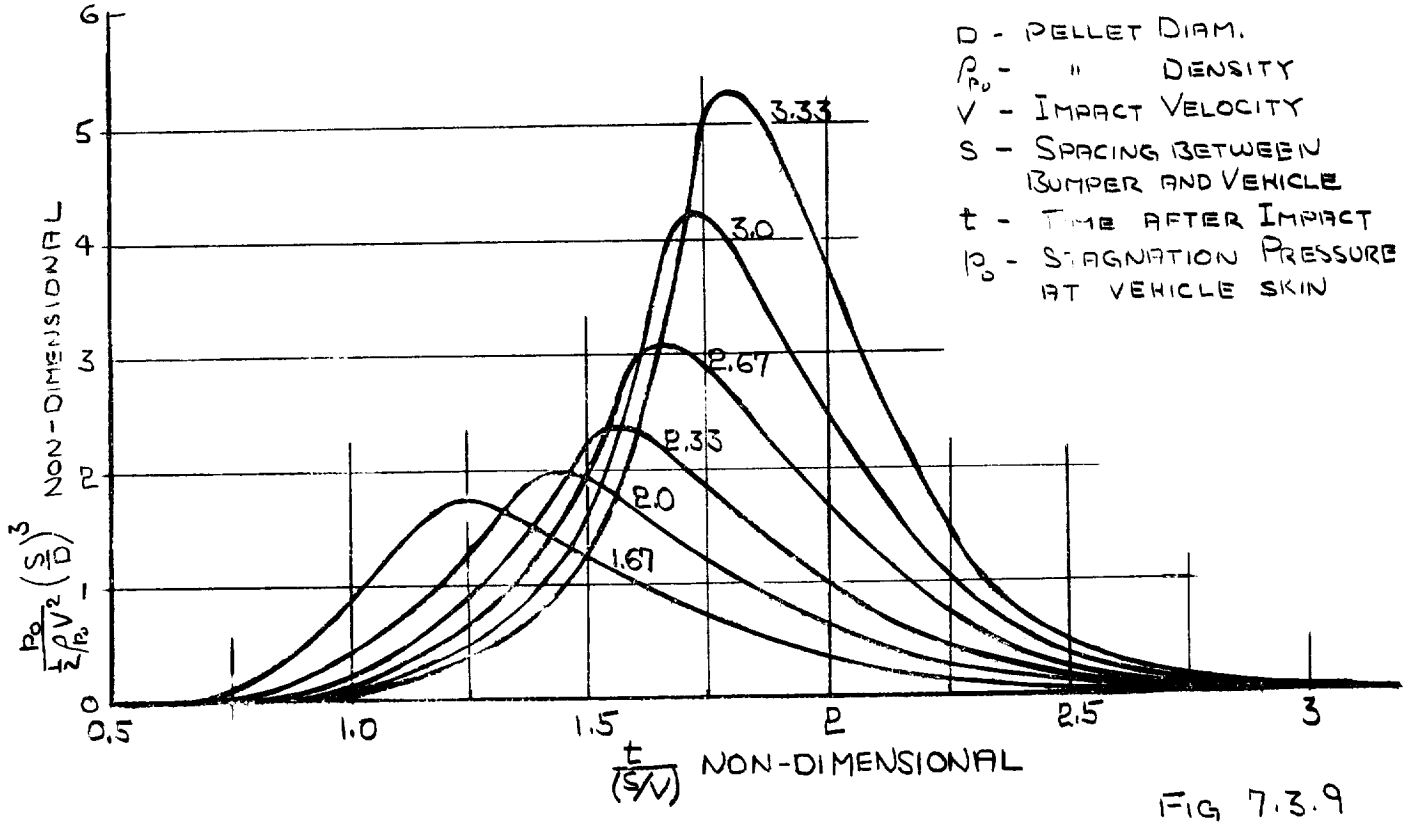

FIG 7.3.9

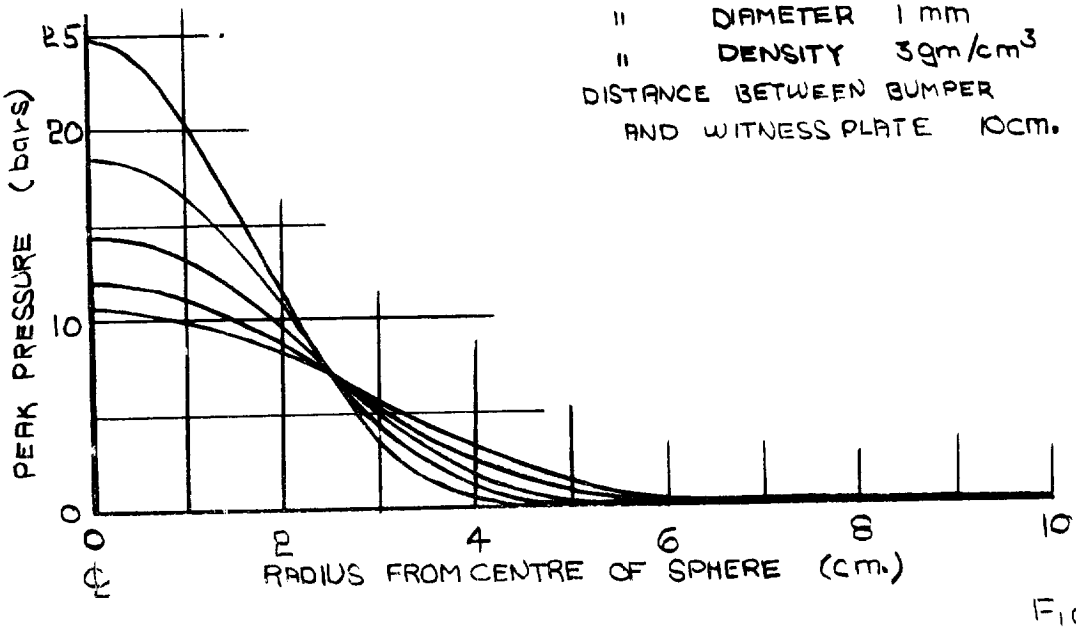

FIG 7.3.10

REFERENCES

1. G.V. Bull
On the Impact of Pellets with Thin Plates.
Theoretical Considerations Part I.
A.D.L. rept. No. 63270-02-01, Jan. 1962.
McGill Tech. Note 1-10/61.

2. Proceedings of the Third Sympositum on Hypervelocity Impact, 1959.

3. Proceedings of the Fourth Symposium on Hypervelocity Impact, 1960.

4. Bjork, R.L.
Effects of Meteoroid Impact on Steel and Aluminum in Space.
The Rand Corporation; p. 1662, December 16, 1958.

5. K.P. Stanyukovich,
The Unsteady Motion of Continuous Media.
Pergamon Press 1961.

6. Cook, M.A., Keyes, R.T.
Microsecond Framing Camera Photographs of High Velocity Impact.
Fluid Symposium, on Hypervelocity Impact 1958.

7. Cook, M.A., McEwan, W.S.
Cohesion in Plasma.
Jour. of App. Phys. V29, n. 11, Nov. 1958 p. 1612.

8. Bauer, A., Cook, M.A., Keyes, R.T.
Detonation generated Plasmas.
Proc. Roy. Soc. A, v. 259. p. 508. 1961.

9. Courant R., Friedrichs, K.O.
Supersonic Flow and Shock Waves.
Interscience Publishers, 1948.

10. Shapiro, A.H.
The Dynamics and Thermodynamics of Compressible Fluid Flow. Ch. 23, 24, 25.
Ronald Press, 1954.

11. Whipple F.L.
The Meteoric Risk To Space Vehicles.
Vistas in Astronautics pp. 115-124.
Pergamon Press, N.Y. 1958.